

Article

# Combustion Metamorphism in Mud Volcanic Events: A Case Study of the 6 May 2000 Fire Eruption of Karabetova Gora Mud Volcano

Svetlana N. Kokh \* and Ella V. Sokol

V.S. Sobolev Institute of Geology and Mineralogy, Siberian Branch Russian Academy of Sciences, 630090 Novosibirsk, Russia

\* Correspondence: zateeva@igm.nsc.ru

**Abstract:** The violent eruption of Karabetova Gora mud volcano on 6 May 2000 (Taman Peninsula, 45°12'16" N; 36°47'05" E) triggered gas ignition as a giant straight-flow vertical gas flare. The 400 m high, short-lived (~15 min) gas flare left no thermal halo on the ground surface, but the thermal shock caused melting or annealing of mud masses which became dispersed in  $\leq 2$  m<sup>3</sup> blocks to distances within 30 m around the volcano conduit. The flare reached the maximum temperatures (~1400–1540 °C) at heights from 75 to 250 m, as estimated by a numerical simulation in SigmaFlow. Bulk melting of dehydrated mud masses was mostly limited to <1.5 cm near the surface of the blocks. Porous paralavas at the site consisted of low- and high-silica K-Al glasses (70%–80%) with residual unmolten grains of detrital quartz and fine (<30 µm) new phases: main intermediate members of the magnetite–ulvöspinel solid solutions and plagioclase (An<sub>45-61</sub>Ab<sub>37-44</sub>Or<sub>2-11</sub> to An<sub>73-90</sub>Ab<sub>10-27</sub>Or<sub>0.5-1</sub>), minor cordierite (X<sub>Fe</sub> = 26%–46%), pigeonite (X<sub>Fe</sub> = 42%–60%), tridymite, cristobalite, and rare mullite. The metapelitic rocks affected by combustion metamorphism were heterogeneous in terms of phase composition and texture. They failed to attain homogeneity due to the high viscosity of anhydrous silicate melts and brevity of the thermal impact. The revealed features of rocks altered by a giant gas fire may serve as a proxy for phase transformation patterns in highly disequilibrium conditions of a thermal shock, far from the formation conditions of ordinary metamorphic rocks.

**Keywords:** mud volcano; eruption; gas ignition; flare; combustion metamorphism; pyrometamorphism; thermal shock; paralava; non-magmatic melts; numerical simulation



**Citation:** Kokh, S.N.; Sokol, E.V. Combustion Metamorphism in Mud Volcanic Events: A Case Study of the 6 May 2000 Fire Eruption of Karabetova Gora Mud Volcano. *Minerals* **2023**, *13*, 355. <https://doi.org/10.3390/min13030355>

Academic Editor: Lifei Zhang

Received: 22 December 2022

Revised: 25 February 2023

Accepted: 28 February 2023

Published: 2 March 2023



**Copyright:** © 2023 by the authors. Licensee MDPI, Basel, Switzerland. This article is an open access article distributed under the terms and conditions of the Creative Commons Attribution (CC BY) license (<https://creativecommons.org/licenses/by/4.0/>).

## 1. Introduction

Generation of voluminous non-magmatic silicate melts in crustal conditions is commonly associated with anatexis and migmatization maintained by heat from deep sources [1–3]. Meanwhile, silicate melts can originate near the surface as well, in the course of combustion metamorphic events, with the heat of burning organic fuel such as bitumen, coal, crude oil, or gas. The temperatures attained during burning of high calorific fuel (up to 900–1600 °C) reach or exceed the level required for melting of dry silicate rocks. As a result, combustion metamorphism (CM) of sedimentary protoliths is often associated with the occurrence of anhydrous melts from high-silica aluminous to high-calcium ultramafic compositions [4–17]. The patterns of generation and crystallization of CM melts derived from sediments, as well as the diversity of the resulting CM rocks, have several controls: the type and amount of combusted fuel (bitumen, coal, oil, or gas); the properties of the sedimentary protoliths (composition, permeability, and bed thickness); and the depth to fire foci. CM complexes produced by coal fires or ignition of bitumen, oil, and gas gushers arise in different geological settings and differ in conditions of metamorphism and in phase composition of its products [4,7–9,12–20].

Combustion metamorphism of sediments affected by burning gas mainly occurs during eruptions of onshore mud volcanoes (MVs). Gas ignition was reported from about

30% of strong MV eruptions, especially frequent in the areas of the Absheron and Taman peninsulas (Azerbaijan and Russia, respectively), Caspian and Azov Seas, Burma, Trinidad, Makran coast, Andaman and Nicobar Islands, Yli basin (Kazakhstan), etc. [13,17,21–24]. The thermal impact of fire eruptions transforms mud masses into diverse CM rocks, from slightly annealed but unmolten rocks via partly fused clinkers, to fully molten paralavas, under temperatures commonly ranging from 900 °C to 1250 °C [13,17], or occasionally up to 1450 °C [7,8,14,25–28]. The strongest alteration involving melting of devolatilized metasedimentary rocks commonly originates in subsurface ignition foci and is spatially limited. Thermally altered sediments are located around the conduit walls [17] or in a net of small fractures [7,8,13,14]. The previous studies of natural and human-caused thermal haloes showed that high-rate gas gushers burn fully in air, with the combustion front above the ground, and can neither form distinct high-temperature metamorphic haloes nor cause sediment melting within their surface projection [16,17].

Karabetova Gora MV in the Taman Peninsula (Black Sea area, southwestern Russia) appears exotic in this context. Its catastrophic eruption on 6 May 2000 triggered gas ignition as a giant 400 m high, short-lived (~15 min) straight-flow vertical gas flare which left no thermal halo on the surface. On the other hand, blocks of mud reaching 2 m<sup>3</sup> in volume dispersed by the explosive eruption were subject to alteration by ultrahigh temperatures within the gas flare core. The alteration conditions approached a thermal shock, while the temperature peaks were several orders of magnitude shorter than in subsurface ignition foci. This is an exceptional or probably unique example of a thermal shock event that has ever occurred in nature.

We describe the features of texture, mineralogy, and geochemistry of the Karabetova Gora combustion metamorphic rocks and use the data to reconstruct the temperature pattern in the flare. The maximum temperatures of thermal alteration were inferred by simulation in SigmaFlow, in a model corresponding to the scenario of a real fire eruption. The modeling revealed the specificity of CM rocks produced by a thermal shock associated with ultrahigh-temperature CM alteration of pelitic sediments under a gas flare.

## 2. Site Description

### 2.1. Karabetova Gora Mud Volcano: Local Geology, Description and Activity History

The Kerch–Taman mud volcanic province lies in a zone of thick Pliocene–Quaternary sediments of the Indol–Kuban Trough extending from the Caucasus foothills through the Taman Peninsula to the Kerch Peninsula. Forty out of eighty mud volcanoes in the province are currently active [23,29–37]. Mud volcanism in the region culminated during the Middle-Late Miocene but has decayed lately. Mud volcanoes, as well as gas fields, in the Kerch and Taman Peninsulas, mainly feed from the Maykop Group shales [23,30–37].

The Karabetova Gora mud volcano is the largest active edifice of the Kerch–Taman MV province located in the southwestern part of the Taman Peninsula between the Kerch strait and the N-S Djiga fault (45°12'16" N; 36°47'05" E), at 147 m above sea level (Figure 1). It lies in the crest of the SW–NE Karabetova fold composed of Eocene–Miocene sediments with the Oligocene–Early Miocene Maykop Group shales in the core [23]. The mud extruded by Karabetova Gora MV mainly consists of the Maykop shale and a minor amount of Upper Miocene (Sarmat stage) clay and marl. The volcanic edifice is a 50 m high, flat-topped, gently sloping hill, ~1.5 km in diameter at the base and about 600 m × 700 m on the top, with a ~250 m main eruptive center (Figure 2a,b) and two satellite centers with several gryphons (Figure 2a,c,d). The activity regime of the main center varies from almost complete dormancy or smooth permanent extrusion of plastic mud, accompanied by episodic moderate gas and mud explosions, to catastrophic eruptions with ignition of gas gushers, extrusion of mud, and diapiric deformation producing large fractures. At least twenty-five large eruptions have occurred since 1818, including four fire events with gas ignition in straight-flow flares [23]. Gryphons from satellite centers are permanently emitting liquid mud, water, and gas (Figure 2c,d).

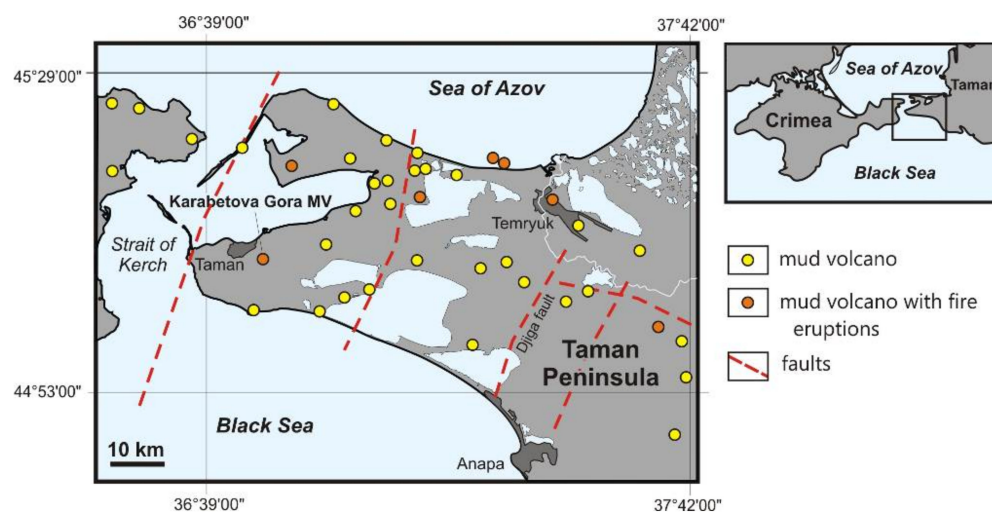


**Figure 1.** Location map of mud volcanoes in the Taman Peninsula (Kerch–Taman MV Province), modified after Shnyukov et al. [23].

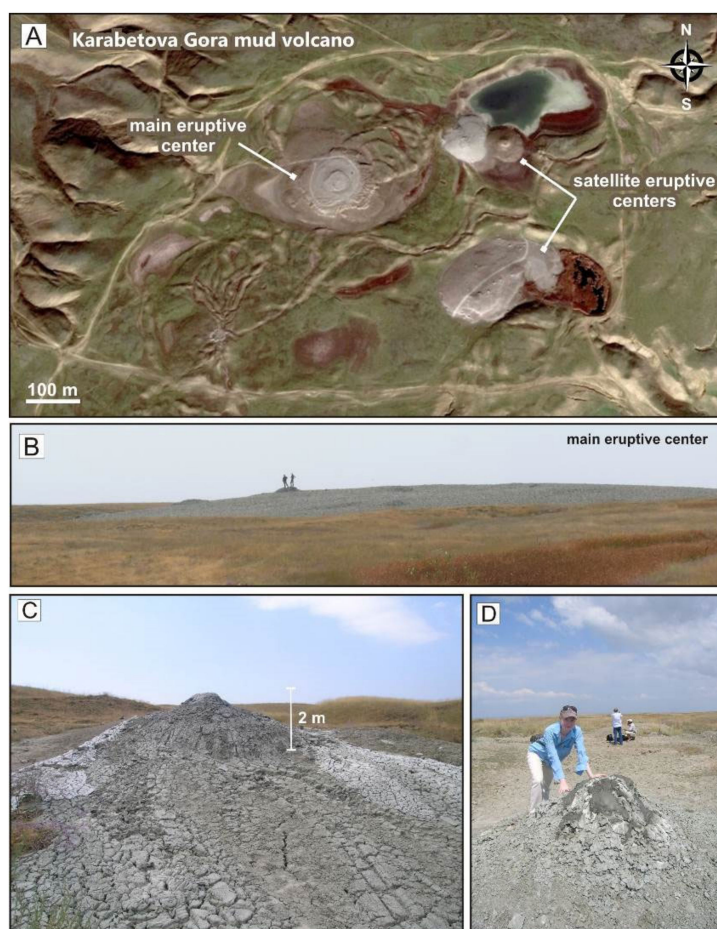


**Figure 2.** Study area and field view of Karabetova Gora MV, August 2008. (A) Panoramic view of Karabetova Gora MV. Google Earth image, 2016 (<https://www.google.com/intl/ru/earth/>, accessed on 5 December 2022). (B) Main eruptive center extruding plastic mud. (C,D) Bubbling satellite gryphons.

Karabetova Gora MV emits methane-dominated gas: 72.2–81.8 vol% CH<sub>4</sub>, 17.7–26.6 vol% CO<sub>2</sub>, 0.53–1.60 vol% N<sub>2</sub>, ≤0.158 vol% Ar, and ≤0.0058 vol% He [31]. Its MV waters have HCO<sub>3</sub>-Cl/Na chemistry and 12.3–14.7 g/L salinity [30,37]. The aqueous fluids are generated

at temperatures  $T_{\text{Mg/Li}} = 80$  to  $89$  °C, as estimated using the Mg/Li geothermometer [38]. With a regional temperature gradient of  $40$  °C/km [39], these temperatures correspond to depths of  $2.0$ – $2.2$  km within the Maykop Group interval [23].

## 2.2. Fire Eruption of 6 May 2000 and Combustion Metamorphic Alteration of Mudrocks

Karabetova Gora MV underwent a catastrophic fire eruption on 6 May 2000 with triggered gas ignition in a  $300$ – $400$  m high flare at the main eruptive center (Figure 3a). According to eye witness reports, the eruption was preceded by an explosion, with an extremely strong boom in the atmosphere and gas ignition afterwards (Stage I).

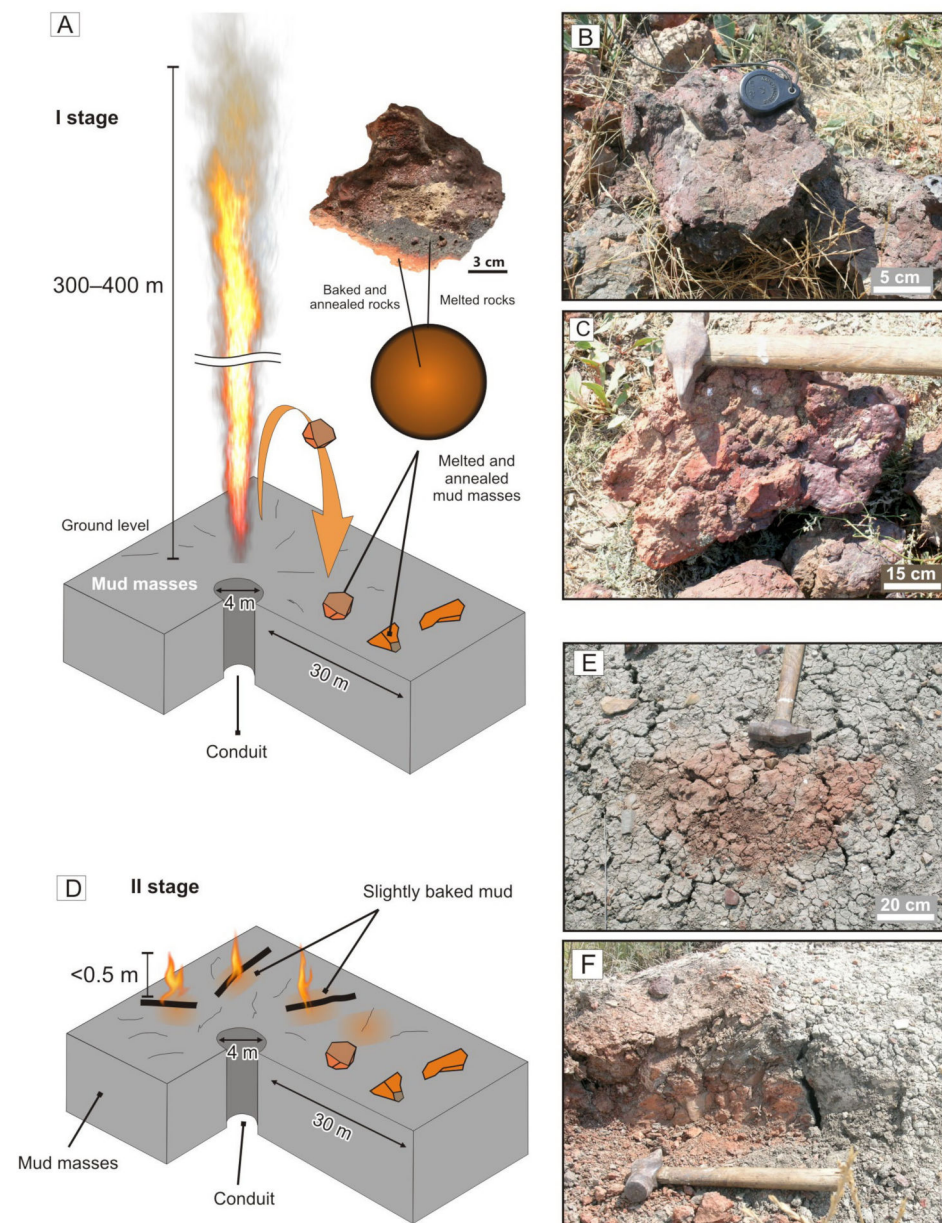


**Figure 3.** Model of Karabetova Gora MV fire eruption of 6 May 2000 and distribution of CM rocks. (A,D) Fire history. Color codes are: gray for unaltered mud; orange for slightly annealed mud and clinker (color intensity is proportional to degree of CM alteration); brown and black for paralava. (B,C) Blocks of clinker and paralava formed upon direct contact with flame (Stage I). (E) Reddish thermally altered rocks around the foci of burning venting gas (Stage II). (F) Reddish annealed mud in heavily fractured mud cover (Stage II).

The burning part of the flare was ball-shaped and radiated a white glow. The exact duration of gas burning is unknown but it hardly exceeded the 15 min average lifespan of gas flares with similar parameters [16,17]. The explosion produced a new 4 m deep crater, 15–20 m in diameter. The ultrahigh-temperature gas flare left no halo around the crater but caused annealing and melting of mud blocks which were thrown up into air from the crater and fell into immediate contact with burning gas. Numerous brick- and scoria-like blocks up to 2 m<sup>3</sup> in size, and many 10 to 30 cm pieces of larger blocks that disintegrated when hit the ground, were dispersed within 30 m around the conduit (Figure 3a–c). All large blocks of annealed and sintered mud have a zoned structure and most of them have an outer zone of black or brownish fused CM rocks with glossy vitrified surfaces and abundant ≤0.5–1 cm round or oval close pores. The highest temperature-fused material (paralava) coated the block surfaces in all samples we analyzed, and melting spots were found no deeper than 2 cm below the block surface. The highest temperature CM rocks apparently lack any veinlets that would record CM melt propagation inward into the blocks but showed sporadic small icicle-like glassy features produced by very limited flow over the block surfaces. The thermal alteration of parent mud rapidly decayed away from the surface, and the rocks in the core are commonly a reddish color, annealed but not fused.

During the active phase of the eruption, mud made up a fractured cover, 30 m in diameter, with gas venting from new fractures. In four hours, the MV conduit (of ~4 m in diameter) was filled with mud masses while the rampart around the crater became dissected by radiating and concentric fractures. Small gas gushers in some of the fractures burned continuously for six days (Stage II; Figure 3d), and their open burning caused slight to moderate thermal effects to the mud: reddening, baking, or rarely sintering. Reddish CM rocks around the foci of burning venting gas often appeared on the walls of open fractures and are local surface marks of deeper burning foci (Figure 3d–f). Most of such foci had been destroyed by the time of our field campaign of 2008, but a few reddish spots are easily recognizable against the background of gray mud (Figure 3e,f).

### 3. Materials and Methods

#### 3.1. Terminology

Combustion metamorphic (pyrometamorphic) rocks are described in this paper with the terminology proposed by Grapes [11], which is used broadly in many overview and other papers concerning these particular rock varieties [12,13,15,40,41]. The terms ‘clinker’ and ‘paralava’ commonly refer to combustion metamorphic (CM) rocks thermally altered to different degrees by coal fires or ignition of bitumen, oil, and gas gushers. ‘Clinkers’ refer to annealed and partially vitrified, variably oxidized, brick-like psammitic–pelitic rocks. ‘Paralavas’ result from extensive fusion and melting of sedimentary rocks and macroscopically resemble vesicular basalt. They sometimes bear flow features of ‘stalactites’, bulbous masses, puddle-like forms, and corrugated micro-flows. Paralavas and vitrified clinkers contain high-temperature (sanidinite facies) minerals and glasses produced by disequilibrium melting and crystallization as a consequence of brief overheating and rapid cooling. Paralavas are considered as partially crystallized and quenched dry non-magmatic silicate melts formed at atmospheric pressure with the ratio of minerals to glass dependent on the melt fraction, rate of cooling, and melt viscosity.

#### 3.2. Sampling

We examined and sampled Karabetova Gora MV during a field trip in August 2008, when it exhibited weak activity and few gryphons spit out small amounts of gassy mud and water. The collection comprised ten samples of extruding fresh and slightly weathered mud masses (liquefied and dry Middle Maykop shale), as well as thirty samples of combustion metamorphic rocks of all types (paralavas, clinkers, and slightly annealed mud). Representative samples from all rock groups, including the sedimentary parent rocks, were subjected to minute mineralogical and geochemical studies.

### 3.3. Analytical Techniques

Analytical procedures were carried out at the Analytical Center for Multielemental and Isotope Research of the Sobolev Institute of Geology and Mineralogy, Russian Academy of Sciences, Siberian Branch (IGM, Novosibirsk, Russia) and the South Ural Research Center of Mineralogy and Geoecology (SU FRC MG, Miass, Russia).

Major elements in bulk rock samples were analyzed by inductively coupled plasma atomic emission spectroscopy (ICP-AES) on a ThermoJarrell IRIS Advantage atomic emission spectrometer (ThermoJarrell Intertech Corporation, Atkinson, WI, USA), at IGM (Novosibirsk, Russia). The preconditioning procedure included fusion of powdered whole-rock samples with lithium borate [42]. The concentrations of Fe(II) and Fe (III) were determined separately by wet chemistry [43].

The ultrafine-grained high-temperature reaction products are difficult to study petrographically but their textures and compositions can be analyzed using back-scattered electron imaging and electron microprobe analysis as main tools for identifying mineral phases and characterizing the reactions. Scanning electron microscopy (SEM) was applied to fragments and thin sections of CM rocks sputter coated with ~15 to 25 nm carbon films. Mineral species were identified using energy-dispersive spectra (EDS), back-scattered electron (BSE) images, and elemental maps (EDS system). The measurements were performed on a Tescan Mira 3MLU scanning electron microscope (Tescan Orsay Holding, Brno, Czech Republic) equipped with an Oxford AZtec Energy Xmax-50 microanalysis system (Oxford Instruments Nanoanalysis, Abingdon, UK) at IGM (Novosibirsk, Russia). The accelerating voltage of 20 kV and 1 nA beam current were used in low- (40–60 Pa) or high-vacuum modes at a 20 s count time.

Electron probe microanalysis (EPMA) with wavelength-dispersive spectrometry (WDS) was used to analyze mineral chemistry of rock-forming and accessory phases on a Jeol JXA 8100 electron microprobe microanalyzer (Jeol Ltd., Tokyo, Japan) in C-coated polished thin sections. Anhydrous minerals were analyzed at an accelerating voltage of 20 kV, a counting time of 10 s, a beam current of 15–30 nA, and a beam diameter of 2–3  $\mu\text{m}$ . Standard samples were synthetic albite for Na, Si, and Al; synthetic diopside for Mg and Ca; natural pyrope O-145 for Fe; synthetic Cl-apatite for P and Cl; phlogopite for F; natural almandine IGM for Mn; natural ilmenite GF-55 for Ti; natural orthoclase 359-1 for K; and synthetic BaSO<sub>4</sub> for S. The detection limits (3 $\delta$  value) for the elements were (in wt%): P and S 0.02; Si, Al, K, and Ca 0.03; Mg, Ti, and Cl 0.04; Fe and Mn 0.06; Na 0.06; and F 0.32. The estimated precision was better than 2% for all major elements and about 5% for trace elements Cl and F.

X-ray diffraction analysis (XRD) was applied to bulk samples of CM rocks, their fragments enriched in crystalline phases, sedimentary parent rocks (mud masses consisting of Middle Maykop shale), and separate clay fractions. Mineral phases ( $\geq 1$  wt%) were identified using a Shimadzu XRD-600 diffractometer (Shimadzu Corporation, Kyoto, Japan) (CuK $\alpha$  radiation with a graphite monochromator,  $\lambda = 1.54178$  Å), at SU FRC MG (Miass, Russia). The scans were recorded from 6 to 60° 2 $\theta$  at 0.05° 2 $\theta$  increments with 5 s scanning time per step. Quantitative mineralogical analysis on the basis of XRD was performed with the Siroquant V 4.1 software package (Sietronics, Mitchell, Australia; license number 11-10419406), using the Siroquant internal crystallographic database for minerals and inorganic materials. The amorphous phase content was also calculated in Siroquant, in samples with an added known amount (15 wt%) of pure corundum Al<sub>2</sub>O<sub>3</sub> as a spike phase. Layered silicates were identified in  $\leq 2$   $\mu\text{m}$  fractions of clay extracted following the method of Hubert et al. [44] from an aqueous suspension of bulk samples using repeated siphoning. X-ray diffraction patterns were recorded for air-dry samples. For precise identification of clay minerals,  $\leq 2$   $\mu\text{m}$  fractions were reanalyzed after being soaked in ethylene glycol for 24 h and heated at 550 °C for 1 h. The air dry (AD), glycolated (EG), and heated (H)  $\leq 2$   $\mu\text{m}$  fractions were repeatedly scanned from 4 to 70° 2 $\theta$  (AD and ED) or 4 to 21° 2 $\theta$  (H).

### 3.4. Approaches to Numerical Simulation

The gas fire during the Karabetova Gora MV eruption of 6 May 2000 was simulated numerically with boundary conditions chosen using available geological and mineralogical data. The distribution of CM rocks was examined in the field, while eye witness reports were referenced to estimate the flare size and to reconstruct both the fire history and the temperature pattern. The conditions of thermal alteration caused by burning methane were inferred from mineralogy and petrology of CM rocks. The simulation was performed for a gusher of methane that blows out from a volcanic conduit and burns in air, while its total (radiative plus convective) heat flux heats up the rocks around the conduit. The models used to simulate processes of this kind account for turbulent flow, turbulent gas combustion, mass motion, and radiative and conductive heat transfer on the surface. The simulation was run in the SigmaFlow software designed jointly by teams from the S.S. Kutateladze Institute of Thermophysics (Novosibirsk, Russia) and the Department of Thermophysics of the Siberian Federal University (Krasnoyarsk, Russia) [45]. The software was tested on a large scope of problems in aerodynamics, heat and mass transfer, and combustion [46]. The approach was applied successfully to gas flare modeling of a Tengiz technological accident in Kazakhstan [16] and Shikhzairli MV fire eruption on 13 March 2011 in Azerbaijan [17].

## 4. Results

### 4.1. Chemistry, Mineralogy and Petrography of Paralavas, Clinkers and Parent Mud Rocks from Karabetova Gora MV

#### 4.1.1. Major-Element Chemistry of Parent Sediments and CM Rocks

A typical mud sample from Karabetova Gora MV contained major oxides of 60.29 wt% SiO<sub>2</sub>, 12.70 wt% Al<sub>2</sub>O<sub>3</sub>, 4.08 wt% FeO, 2.13 wt% Fe<sub>2</sub>O<sub>3</sub>, 2.98 wt% Na<sub>2</sub>O, 1.79 wt% K<sub>2</sub>O, and 1.80 wt% MgO (Table 1), with low CaO (1.86 wt%), TiO<sub>2</sub> (0.78 wt%), P<sub>2</sub>O<sub>5</sub> (0.16 wt%), and MnO (0.09 wt%) contents at loss on ignition (LOI) as high as 10.89 wt%. The thermally altered Karabetova Gora mud breccia was dehydrated CM rock (LOI from 0.42 to 1.21 wt%) with high contents of SiO<sub>2</sub> (62.6–63.5 wt%), Al<sub>2</sub>O<sub>3</sub> (18.2–19.2 wt%), and K<sub>2</sub>O (2.5–2.8 wt%) (Table 1). Na<sub>2</sub>O is 1.0–1.5 wt%; iron contents (FeO + Fe<sub>2</sub>O<sub>3</sub>) range from 7 to 9 wt%. Other oxides include MgO (2.3–2.5 wt%), CaO (1.2–2.1 wt%), TiO<sub>2</sub> (~1 wt%), and MnO (~0.1 wt%). The composition difference of CM rocks from the precursor sediments (Figure 4) was highlighted by normalizing the element contents to those in dry mud. Compared to the dehydrated protolith composition, the CM rocks showed enrichment in Al<sub>2</sub>O<sub>3</sub> (3–5 wt%), slight enrichment in K<sub>2</sub>O (0.7–0.8 wt%) and MgO (0.3–0.5 wt%), depletion in SiO<sub>2</sub> (4.2–4.7 wt%) and Na<sub>2</sub>O (1.8–2.4 wt%), and comparable contents of TiO<sub>2</sub>, MnO, and P<sub>2</sub>O<sub>5</sub>, according to mass balance calculations. The large range of CaO contents is due to the original heterogeneity in the distribution of Ca carbonates (mainly fossils) in the Maykop shales. The Fe<sup>2+</sup> compounds were more abundant than those of Fe<sup>3+</sup> in black CM rocks (FeO/Fe<sub>2</sub>O<sub>3</sub> = 3.3–4.6) but less abundant (FeO/Fe<sub>2</sub>O<sub>3</sub> = 0.16–0.42) in brownish and reddish varieties. The variance of FeO/Fe<sub>2</sub>O<sub>3</sub> ratios in CM rocks was also evident in the pattern (Figure 4) normalized to the sedimentary protolith with the initial FeO/Fe<sub>2</sub>O<sub>3</sub> = 1.92.

#### 4.1.2. Mineralogy of CM Rocks and their Sedimentary Protolith

The sedimentary protolith of the sampled CM rocks mainly consisted of illite–smectite (37 wt%), quartz (16 wt%), chlorite (15 wt%), and micas (predominant muscovite and sporadic biotite, 15 wt% in total), with small percentages of plagioclase (6 wt%), pyrite (4 wt%), gypsum (4 wt%), and calcite (3 wt%). The relative percentages of clay minerals in the ≤2 μm fraction, as well as the patterns of mixed-layer phases, were determined by XRD in representative mud samples (Middle Maykop shale).

The blocks of thermally altered mud are often zoned. The strongest thermal alteration (with patches of bulk or spotty melting) penetrated no deeper than 1.5 cm below the surface of the blocks.

Paralavas at the site were vesicular aphanitic rocks that look like artificial slag, with oval isolated pores. The rocks were mainly composed of brownish or blackish moderate

to high-silica K-Al glass (70–80 wt%) (Table 2, Figure 5a). The glass enclosed unmolten round relict detrital grains of quartz (6–16 wt%) and ultrafine (<5 μm) newly formed grains (<20 wt%), occasionally up to 30 μm (Figures 5–7). They were mostly ferrous spinel and plagioclase, as well as some cordierite and tridymite. One paralava sample contained clinopyroxene (Table 2). Most of bulk paralava samples bore up to 2 wt% cristobalite (revealed by XRD) but only one sample contained mullite, despite quite high Al<sub>2</sub>O<sub>3</sub> content in the rocks. The newly formed phases were unevenly distributed in paralavas and appeared in clusters as evidence of the original micro-heterogeneity of the precursor sediments (Figure 5d, Figure 6b,d, and Figure 7c).

**Table 1.** Major-element compositions (in wt%) of typical combustion metamorphic rocks and representative unaltered mud samples from Karabetova Gora MV (Taman Peninsula).

Rock Type	Mud	Combustion Metamorphic Rocks					
Sample	08-12-13	KG-3	KG-4	08-12-1	08-12-5	08-12-10	08-12-12
Rock color		black	black	black	red-brown	red-brown	black-brown
SiO <sub>2</sub>	60.29	62.89	63.45	62.62	62.73	62.70	63.08
TiO <sub>2</sub>	0.78	0.95	0.98	0.97	0.96	0.98	0.97
Al <sub>2</sub> O <sub>3</sub>	12.70	18.15	18.45	18.80	18.15	18.80	19.20
Fe <sub>2</sub> O <sub>3</sub>	2.13	1.93	1.99	1.44	6.58	7.73	3.63
FeO	4.08	6.55	6.60	6.68	2.75	1.24	4.83
MnO	0.09	0.11	0.11	0.10	0.11	0.10	0.09
MgO	1.80	2.42	2.35	2.49	2.38	2.33	2.29
CaO	1.86	1.50	1.30	2.10	1.20	1.30	1.20
Na <sub>2</sub> O	2.98	1.52	1.41	0.94	0.99	1.28	1.35
K <sub>2</sub> O	1.79	2.84	2.79	2.72	2.81	2.78	2.75
P <sub>2</sub> O <sub>5</sub>	0.16	0.19	0.14	0.17	0.14	0.13	0.14
LOI	10.89	0.48	0.42	0.98	1.21	0.76	0.63
S <sub>total</sub>	<0.05	0.10	0.06	<0.05	<0.05	<0.05	<0.05
Total	99.55	99.63	100.05	100.01	100.01	100.13	100.16
FeO/Fe <sub>2</sub> O <sub>3</sub>	1.92	3.39	3.31	4.63	0.42	0.16	1.33

LOI = loss on ignition.

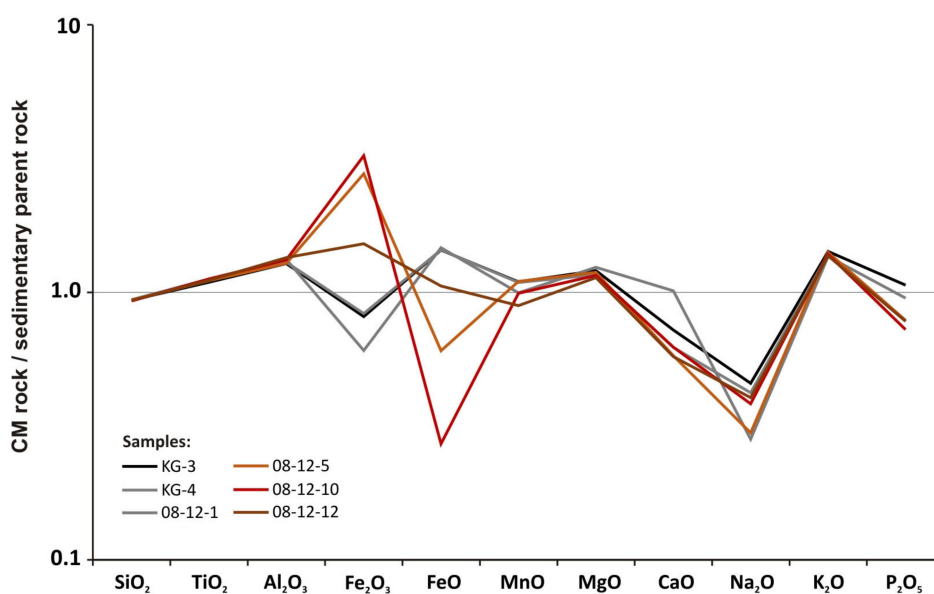


**Figure 4.** Major-element patterns for the Karabetova Gora CM rocks normalized to protolith composition (mud composed of Middle Maykop shale), based on data from Table 1.

**Table 2.** Mineral assemblages in metapelitic combustion metamorphic rocks from Karabetova Gora MV (Taman Peninsula) determined by XRD.

Sample	KG-3	KG-4	08-12-1	08-12-5	08-12-5	08-12-10	08-12-12
Rock	p	p	p	p	cl	p	p
Glass	74	70	73	71	74	80	76
Plagioclase	5	5	4	4	2	1	2
Cordierite	3	1	2				†
Pigeonite	3						
Cristobalite	<1		1	1	1	<1	2
Tridymite	†		†				†
Mullite						†	
Ferrous spinel	9	11	9	7	3	†	9
Magnesioferrite	†					2	
Ilmenite	†						
Hematite				2	5	8	2
Pyrite *	†						
Quartz *	6	13	11	16	16	10	9

p = paralava; cl = clinker; \* relict detrital minerals. XRD data in wt%; †: single grains identified by SEM-EDS and EPMA.

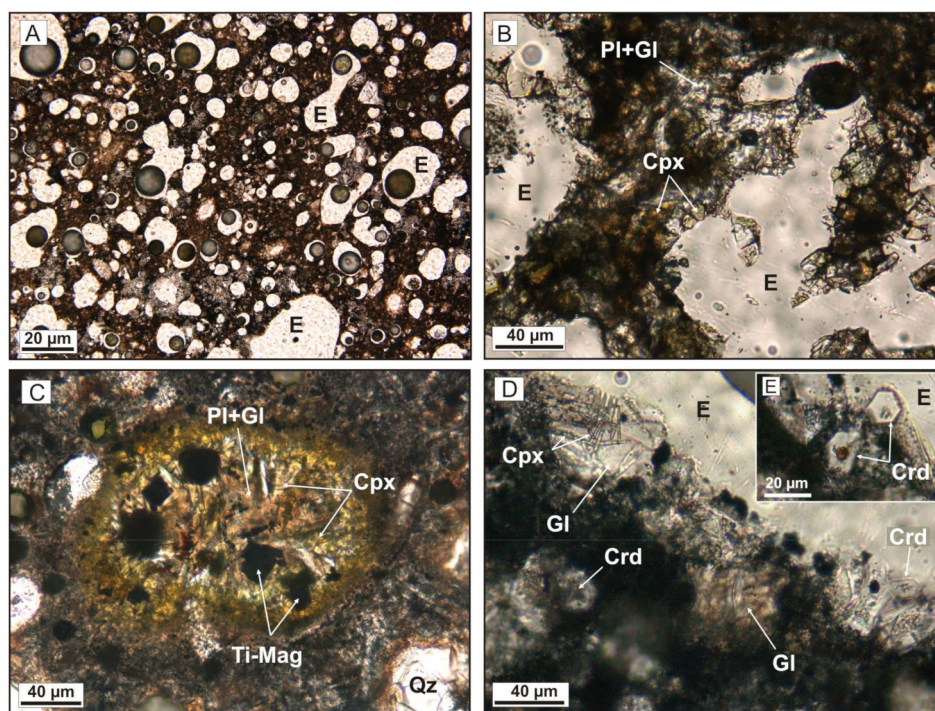


**Figure 5.** Photomicrographs (plane-polarized light) of paralava thin sections. (A) Paralava with abundant oval and elongate vesicles occupied by epoxy resin. (B) Pigeonite crystals and plagioclase laths in brown glass. (C) Cluster of ferrous spinel and pigeonite crystals with glass and plagioclase laths. (D,E) Prismatic Fe-rich cordierite and pigeonite laths buried in brown and colorless siliceous Al-K-rich glass. Crd = cordierite, Cpx = pigeonite, Gl = glass, E = epoxy resin, Pl = plagioclase, Qz = quartz, Ti-Mag = intermediate members of the magnetite-ulvöspinel solid solutions.

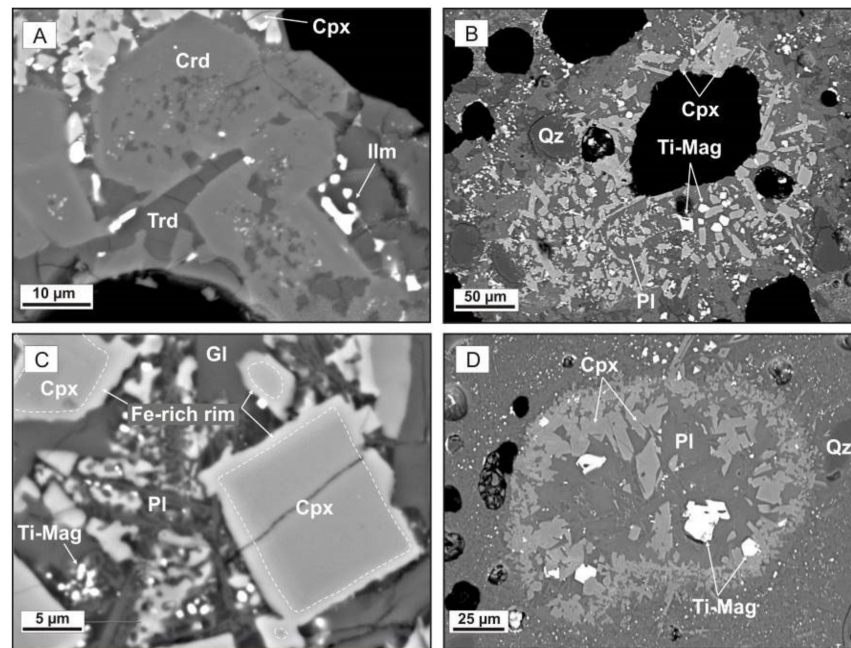


**Figure 6.** BSE images of newly formed aluminosilicate minerals from paralavas. (A) Aggregate of prismatic Fe-rich cordierite crystals with tridymite inclusions, tridymite laths, zoned pigeonite crystals, and ilmenite globules. (B) Pigeonite crystals and ferrous spinel isometric and hopper-like crystals localized in a glass matrix around pores. Undermolten relict detrital quartz grains with perlitic cracks. (C) Zoned pigeonite crystals and plagioclase laths in siliceous Al-K-rich glass. (D) Cluster of ferrous spinel and pigeonite crystals, and plagioclase laths. Crd = cordierite, Cpx = pigeonite, Gl = glass, Ilm = ilmenite, Pl = plagioclase, Qz = quartz, Ti-Mag = intermediate members of the magnetite–ulvöspinel solid solutions, Trd = tridymite.

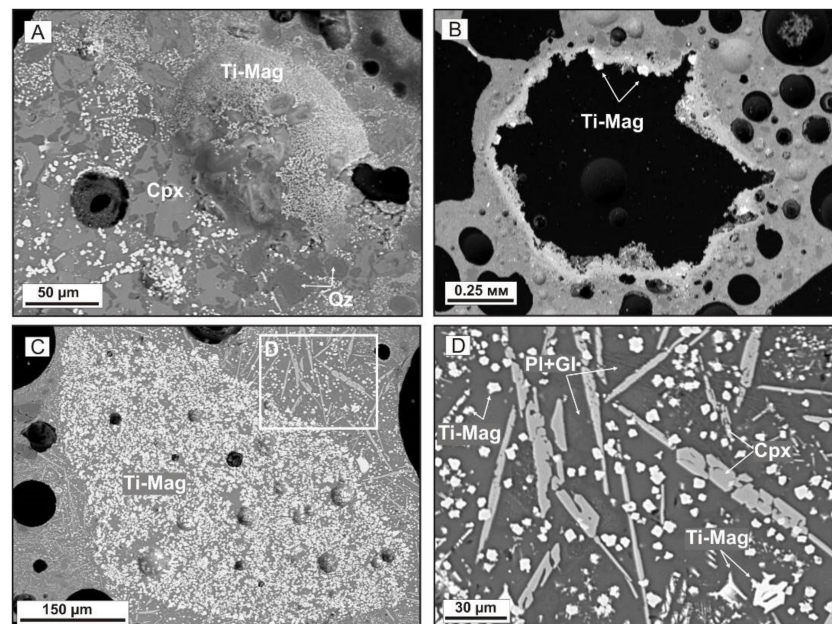


**Figure 7.** Morphology of ferrous spinel from MV paralavas. (A) Inner surface of an open pore in a glass matrix encrusted with pigeonite and ferrous spinel. (B) Pore in a glass matrix rimmed by ferrous spinel. (C) Cluster of ferrous spinel crystals. (D) Newly formed elongate hopper-like crystals of pigeonite and isometric and hopper crystals of ferrous spinel in a glass matrix with abundant plagioclase laths. BSE images. Cpx = pigeonite, Gl = glass, Pl = plagioclase, Qz = quartz, Ti-Mag = intermediate members of the magnetite–ulvöspinel solid solutions.

Tridymite occurred as thin elongate laths (within 30  $\mu\text{m}$  long) or anhedral grains, or as inclusions in cordierite (Figure 6a). Tridymite in the Karabetova Gora samples never formed imbricate interstitial aggregates unlike that in coal fire paralavas. The mineral was easily identified by its habit and lilac fluorescence under the microprobe beam, and its presence is confirmed by X-ray powder diffraction ( $d/N$  ( $\text{\AA}$ ): 4.318, 4.092, 3.819, and 2.496) of small rock fragments enriched in this phase. The chemistry of the tridymite is briefly described below (Section 4.2). Cristobalite was identified by X-ray powder diffraction only, from an intense reflection ( $I = 100$ ) at  $d/N = 4.040$   $\text{\AA}$  and two much weaker reflections at (3.515 and 2.487  $d/N$  ( $\text{\AA}$ )).

Like other  $\text{SiO}_2$  polymorphs, relict detrital quartz in clinker and paralava was determined by XRD (main reflections at 4.251, 3.348, and 1.817  $d/N$  ( $\text{\AA}$ )) and was detectable from its optic properties, morphology (undigested sandy grains), and bright blue fluorescence under an electron beam.

Cordierite often occurred as tiny ( $<20$   $\mu\text{m}$ ) pseudo-hexagonal short-prismatic crystals lining the walls of gas vesicles (Figure 5d,e and Figure 6a) or appeared as prismatic crystals and anhedral grains in the groundmass. In the latter case, it had cores stuffed with tridymite and glass inclusions but the cordierite that grew around vugs virtually lacks inclusions. These morphological features are typical of CM cordierite [11,12,15,47]. Clinopyroxene existed as flat 5–20  $\mu\text{m}$  crystals (Figure 6b–d), anhedral grains, or skeletal and hopper crystals (Figures 5d and 7d). Plagioclase formed laths or anhedral grains set in glass, while its clusters were mostly abundant in the glassy matrix on the block surfaces (Figure 5b,c and Figure 6c,d). Opaque minerals in the paralavas were intermediate members of the magnetite–ulvöspinel solid solutions, magnetite–magnesian ferrite solid solution series, and ilmenite (Figure 5c, Figure 6a,d, and Figure 7). Fine aggregates of opaque minerals were localized in the outer zone most strongly affected by the thermal impact, within 1.5 cm below the surface. Skeletal and/or hopper crystals of opaque phases clustered on the periphery of pores (Figure 7a,b) or in thin bridges between them.

Annealed hardened material akin to brick, was impregnated with fine hematite retaining the original texture patterns of the mud breccia, and was coated with a thin ( $\leq 2.0$  cm) crust of paralava. Under the paralava crust, the thermally altered rocks enclosed unmolten relict detrital grains of quartz and, less often, high-silica plagioclase. The pattern of pores is irregular while the pores themselves have intricate shapes. These rocks contain dehydrated, dehydroxylated, and mostly X-ray amorphous phyllosilicates (as a result of thermally induced solid-state amorphization), while no high-temperature phases appeared (Figure S1).

The XRD patterns of the sedimentary protolith and CM rocks showed evolution of their phase compositions upon annealing and melting (Figure S1). Slightly annealed rocks become devoid of gypsum and calcite, retained a dehydroxylated illite-like phyllosilicates marked by a 10  $\text{\AA}$  diffraction peak, and acquired hematite. Clinkers lacked the phyllosilicates but bore higher percentages of hematite which was absent from black paralavas. New phases in CM rocks were cristobalite in clinker and cordierite in paralavas. Ferrous spinel appeared in clinker and showed up as a notably larger main diffraction peak in the higher-temperature paralavas. Quartz was present in all CM rocks and in their sedimentary protolith, and its contents decreased progressively with increasing CM alteration temperatures, down to 6 wt% in paralavas. The presence of an amorphous phase (vitreous in paralavas) was detectable from a higher background in X-ray diffraction patterns. The XRD patterns of both clinkers and paralavas showed broad haloes from 20 to 30°  $2\theta$  (Figure S1).

#### 4.2. Chemistry of Minerals and Glasses in the Karabetova Gora Paralavas

Glasses with inclusions of newly formed phases were anhydrous and had intermediate to high-silica compositions. They were highly heterogeneous and contained 61.5 to 75.7 wt%  $\text{SiO}_2$ , 14.1 to 23.2 wt%  $\text{Al}_2\text{O}_3$ , 2.3 to 6.1 wt% Fe, 2.6 to 4.9 wt%  $\text{K}_2\text{O}$ , 0.5 to 2.5 wt%  $\text{Na}_2\text{O}$ , and 0.3 to 1.6 wt% MgO (Table 3); MnO and  $\text{P}_2\text{O}_5$  were below 0.1 and 0.3 wt%, respectively. The large ranges of major oxides mirrored the microheterogeneity of the precursor sediment,

with clusters of quartz or feldspar grains, mica and hydromica particles, carbonates, iron oxides and/or sulfides. Relict detrital quartz grains were rimmed by high-silica glass with 80.3–86.3 wt% SiO<sub>2</sub> (Table 3).

**Table 3.** Compositions of glass in combustion metamorphic rocks from Karabetova Gora MV (Taman Peninsula). EPMA data (in wt%).

Location	Glass from Interstitial Space between Newly Formed Phases										Rims around Relict Detrital Quartz Grains		
SiO <sub>2</sub>	61.54	61.85	62.67	64.36	68.85	72.09	72.41	72.98	73.72	75.66	80.31	84.45	86.27
TiO <sub>2</sub>	0.32	0.25	0.54	0.20	0.87	0.51	0.43	0.04	0.43	0.82	0.51	0.79	0.38
Al <sub>2</sub> O <sub>3</sub>	23.18	22.80	21.00	21.41	15.57	16.37	15.77	15.71	14.88	14.13	10.45	7.90	8.72
FeO	5.25	4.21	6.10	3.92	5.03	3.27	2.88	2.85	2.60	2.26	3.63	1.39	2.22
MnO	0.09	0.12	0.11	0.09	0.07	0.09	0.07	0.07	0.07	<0.06	<0.06	<0.06	<0.06
MgO	0.27	1.42	0.55	0.28	0.85	1.00	1.56	1.07	1.36	0.84	0.19	0.71	0.28
CaO	5.30	6.23	4.06	7.17	1.44	0.63	0.42	0.51	0.45	0.52	1.96	0.22	1.88
Na <sub>2</sub> O	0.61	0.61	0.79	0.51	2.46	1.22	1.21	1.42	1.21	1.08	0.34	1.07	0.30
K <sub>2</sub> O	3.14	2.55	3.47	2.65	3.66	4.50	4.55	4.69	4.85	4.65	0.18	2.93	0.09
P <sub>2</sub> O <sub>5</sub>	0.26	0.08	0.34	0.04	0.10	0.03	<0.02	0.04	0.07	0.03	0.51	0.07	0.06
Total	99.96	100.11	99.62	100.64	98.90	99.70	99.31	99.38	99.63	100.00	98.09	99.51	100.19

Clinopyroxene was aluminous pigeonite with X<sub>Fe</sub> from 42 to 60% (Table 4) and with notable enrichment in MnO (up to 7.4 wt%). The clinopyroxene crystals had prominent chemical zoning, with little variable MgO (11.1 to 12.3 wt%) but a marked core–rim difference in FeO and CaO: 24.8 wt% (rim) against 10.6 wt% (core) FeO and 5.7 wt% (rim) against 17.7 wt% (core) CaO. Such sharp zonation is quite often observed in pyroxenes from CM rocks, especially in mineral grains that formed during rapid cooling [48–50].

**Table 4.** Mineral chemistry of clinopyroxene from combustion metamorphic rocks of Karabetova Gora MV. EPMA data (in wt%).

Analysis No.	1	2	3	4	5	6	7 Core	8 Rim	9 Rim
SiO <sub>2</sub>	50.16	51.34	51.31	50.70	51.76	51.00	51.70	50.84	51.28
TiO <sub>2</sub>	0.30	0.28	0.31	0.32	0.20	0.40	0.38	0.38	0.33
Al <sub>2</sub> O <sub>3</sub>	6.37	8.24	4.00	3.89	1.85	1.93	2.38	1.23	2.08
FeO	18.70	16.94	18.15	18.86	19.68	22.28	10.60	24.78	24.27
MnO	6.52	5.85	7.40	6.83	5.92	0.33	5.33	5.03	5.05
MgO	12.39	11.86	14.78	16.13	17.53	17.56	11.90	12.27	11.07
CaO	5.62	5.37	4.52	3.58	3.55	7.02	17.67	5.70	6.23
Na <sub>2</sub> O	0.18	0.50	0.16	0.08	0.09	<0.06	0.16	<0.06	0.18
K <sub>2</sub> O	<0.03	0.09	0.04	<0.03	<0.03	<0.03	<0.03	<0.03	<0.03
Total	100.26	100.46	100.66	100.40	100.60	100.56	100.13	100.23	100.50
	6 oxygen atoms, apfu								
Si	1.906	1.916	1.940	1.922	1.958	1.928	1.958	1.983	1.989
Ti	0.009	0.008	0.009	0.009	0.006	0.011	0.011	0.011	0.010
Al	0.285	0.363	0.178	0.174	0.082	0.086	0.106	0.057	0.095
Fe	0.594	0.529	0.574	0.598	0.623	0.704	0.336	0.808	0.787
Mn	0.210	0.185	0.237	0.219	0.190	0.011	0.171	0.166	0.166
Mg	0.702	0.660	0.833	0.911	0.988	0.990	0.672	0.713	0.640
Ca	0.229	0.215	0.183	0.145	0.144	0.284	0.717	0.238	0.259
Na	0.013	0.036	0.011	0.006	0.006	0.000	0.012	0.000	0.013
K	0.000	0.004	0.002	0.000	0.000	0.000	0.000	0.000	0.000
Total	3.947	3.915	3.968	3.985	3.997	4.014	3.983	3.977	3.959
	End members								
Mg <sub>2</sub> Si <sub>2</sub> O <sub>6</sub>	46.03	47.02	52.38	55.08	56.32	50.03	38.96	40.54	37.96
Ca <sub>2</sub> Si <sub>2</sub> O <sub>6</sub>	15.01	15.29	11.52	8.78	8.20	14.37	41.58	13.53	15.35
Fe <sub>2</sub> Si <sub>2</sub> O <sub>6</sub>	38.96	37.69	36.10	36.14	35.48	35.60	19.47	45.93	46.68
X <sub>Fe</sub> , %	53.39	51.96	49.34	47.28	45.12	41.94	42.99	57.73	59.82

apfu = atoms per formula unit; X<sub>Fe</sub> = (Fe + Mn)/(Fe + Mn + Mg) × 100%. P<sub>2</sub>O<sub>5</sub> < 0.02 wt%.

Newly formed plagioclase was labradorite (An<sub>45–61</sub>Ab<sub>37–44</sub>Or<sub>2–11</sub>) and bytownite (An<sub>73–90</sub>Ab<sub>10–27</sub>Or<sub>0.5–1</sub>) (Table 5). The amount of K<sub>2</sub>O was from 0.08 to 1.59 wt%; FeO reached 1.31–1.40 wt% in bytownite but was slightly lower (0.45–0.89 wt%) in labradorite varieties.

**Table 5.** Mineral chemistry of plagioclase from combustion metamorphic rocks of Karabetova Gora MV. EPMA data (in wt%).

Analysis No.	1	2	3	4	5	6
SiO <sub>2</sub>	61.97	53.94	54.18	55.29	50.81	51.50
TiO <sub>2</sub>	0.26	0.11	0.14	0.20	0.04	0.09
Al <sub>2</sub> O <sub>3</sub>	23.43	28.96	28.96	26.86	30.31	30.33
FeO	0.89	0.45	0.47	1.21	1.31	1.40
MnO	0.21	0.18	0.16	0.08	<0.06	0.14
CaO	7.36	11.73	11.79	13.22	14.84	15.04
Na <sub>2</sub> O	4.01	4.05	3.98	2.65	2.56	0.92
K <sub>2</sub> O	1.59	0.33	0.34	0.17	0.15	0.08
P <sub>2</sub> O <sub>5</sub>	0.05	<0.02	<0.02	0.05	<0.02	<0.02
Total	99.77	99.74	100.01	99.71	100.07	99.50
			8 oxygen atoms, apfu			
Si	2.761	2.445	2.449	2.508	2.324	2.353
Ti	0.009	0.004	0.005	0.007	0.001	0.003
Al	1.230	1.547	1.543	1.436	1.634	1.633
Fe	0.033	0.017	0.018	0.046	0.050	0.054
Mn	0.008	0.007	0.006	0.003	0.000	0.005
Ca	0.351	0.570	0.571	0.643	0.727	0.736
Na	0.347	0.356	0.349	0.233	0.227	0.081
K	0.090	0.019	0.020	0.010	0.009	0.004
P	0.002	0.000	0.000	0.002	0.000	0.000
Total	4.831	4.965	4.959	4.886	4.972	4.870
			End members			
CaAl <sub>2</sub> Si <sub>2</sub> O <sub>8</sub>	44.55	60.29	60.79	72.58	75.56	89.56
NaAlSi <sub>3</sub> O <sub>8</sub>	43.99	37.69	37.12	26.29	23.55	9.91
KAlSi <sub>3</sub> O <sub>8</sub>	11.47	2.02	2.09	1.14	0.89	0.53

apfu = atoms per formula unit; MgO < 0.05 wt%.

Cordierite ( $X_{\text{Fe}} = 26\text{--}46\%$ ) showed an Al deficit (3.45–3.90 apfu) and Si excess (5.05–5.42 apfu) relative to the stoichiometric composition (Table 6). The channel positions had low occupation by cations, and the content of potassium was higher than sodium: 0.02–0.06 apfu K, 0.16–0.49 wt% K<sub>2</sub>O and 0.02 apfu Na, 0.03–0.12 wt% Na<sub>2</sub>O. High totals in the EPMA data (100.3 wt% on average) indicate very low contents of volatiles (H<sub>2</sub>O, CO<sub>2</sub>). In general, the morphology and chemistry features of Fe-enriched cordierite from the Karabetova Gora paralavas were similar to other CM cordierites from coal fire settings [9,10,12,47,49,51].

Unlike unmolten relict detrital quartz with ~99.8 wt% SiO<sub>2</sub>, tridymite contained ubiquitous impurities reaching 3.5–5.6 wt% in total (Table 7), especially 1.7–3.4 wt% Al<sub>2</sub>O<sub>3</sub>, 0.2–1.3 wt% FeO, and within 0.7 wt% K<sub>2</sub>O, which is typical of tridymite from CM rocks [5,9,10,12,47,52]. Other oxides were present frequently but in smaller amounts: Na<sub>2</sub>O (0.3–0.5 wt%), MgO (≤0.4 wt%), and TiO<sub>2</sub> (≤0.4 wt%).

Ferrous spinel had an intermediate composition of the magnetite–ulvöspinel solid solutions, with considerable amounts of Al<sub>2</sub>O<sub>3</sub> (4.2–13.3 wt%) (Table 8); it also contained 0.4–0.6 wt% MnO and 0.7–1.2 wt% CaO. Ilmenite bore minor amounts of MgO (≤3.2 wt%), Al<sub>2</sub>O<sub>3</sub> (≤2.4 wt%), MnO (≤0.9 wt%), and SiO<sub>2</sub> (≤0.4 wt%).

**Table 6.** Mineral chemistry of Fe-enrich cordierite from combustion metamorphic rocks of Karabetova Gora MV. Representative and average compositions. EPMA data (in wt%).

Analysis No.	1	2	3	4	Mean n = 14	S	Min	Max
SiO <sub>2</sub>	50.40	49.77	48.98	49.94	50.54	0.74	48.98	52.12
TiO <sub>2</sub>	0.18	0.16	0.18	0.17	0.18	0.05	0.11	0.31
Al <sub>2</sub> O <sub>3</sub>	32.48	32.79	32.53	32.59	31.85	0.73	30.46	32.79
FeO	6.73	7.16	9.44	10.28	7.66	1.09	6.47	10.28
MnO	0.12	0.12	0.15	0.17	0.14	0.02	0.11	0.17
MgO	10.07	10.13	8.34	6.96	9.39	0.91	6.96	10.41
CaO	0.05	0.06	0.07	0.09	0.09	0.05	0.05	0.19
Na <sub>2</sub> O	0.06	0.07	0.06	0.12	0.07	0.03	0.03	0.12
K <sub>2</sub> O	0.26	0.20	0.20	0.24	0.27	0.09	0.16	0.49
P <sub>2</sub> O <sub>5</sub>	0.05	0.04	0.18	0.13	0.08	0.05	<0.02	0.18
Total	100.41	100.51	100.13	100.68	100.26	0.44	99.27	100.91
18 oxygen atoms, apfu								
Si	5.051	4.996	4.986	5.064	5.091	0.063	4.986	5.223
Ti	0.013	0.012	0.014	0.013	0.013	0.004	0.008	0.023
Al	3.837	3.880	3.903	3.895	3.782	0.090	3.598	3.903
Fe	0.564	0.601	0.803	0.872	0.645	0.095	0.544	0.872
Mn	0.011	0.010	0.013	0.014	0.012	0.002	0.009	0.014
Mg	1.505	1.516	1.265	1.052	1.410	0.134	1.052	1.560
Ca	0.006	0.007	0.008	0.010	0.010	0.005	0.005	0.020
Na	0.009	0.013	0.011	0.023	0.014	0.006	0.006	0.023
K	0.034	0.026	0.026	0.031	0.034	0.011	0.021	0.063
P	0.004	0.004	0.016	0.011	0.007	0.004	0.001	0.016
Total	11.033	11.066	11.045	10.986	11.019	0.027	10.964	11.066
End members								
Mg <sub>2</sub> Al <sub>4</sub> Si <sub>5</sub> O <sub>18</sub>	72.35	71.27	60.76	54.28	68.13	5.32	54.28	73.77
Fe <sub>2</sub> Al <sub>4</sub> Si <sub>5</sub> O <sub>18</sub>	27.14	28.25	38.60	44.98	31.31	5.25	25.70	44.98
Mn <sub>2</sub> Al <sub>4</sub> Si <sub>5</sub> O <sub>18</sub>	0.51	0.47	0.63	0.74	0.56	0.09	0.45	0.74
X <sub>Fe</sub> , %	27.65	28.73	39.24	45.72	31.87	5.32	26.23	45.72

apfu = atoms per formula unit; n = number of samples; mean = mean value; S = standard deviation; min = minimum value; max = maximum value; X<sub>Fe</sub> = (Fe + Mn)/(Fe + Mn + Mg) × 100%.

**Table 7.** Mineral chemistry of tridymite from combustion metamorphic rocks of Karabetova Gora MV. EPMA data (in wt%).

Analysis No.	1	2	3	4	5	6
SiO <sub>2</sub>	94.20	94.25	94.35	95.55	95.94	96.46
TiO <sub>2</sub>	0.24	0.22	0.41	0.45	0.12	0.30
Al <sub>2</sub> O <sub>3</sub>	2.66	3.43	2.32	1.79	2.32	1.91
FeO	1.25	0.24	1.33	0.31	0.82	0.39
MgO	0.11	0.05	0.27	0.05	0.40	0.25
CaO	0.32	1.21	0.18	0.60	0.09	0.12
Na <sub>2</sub> O	0.28	0.51	0.37	0.30	0.30	0.31
K <sub>2</sub> O	0.66	<0.03	0.05	0.29	0.10	0.16
P <sub>2</sub> O <sub>5</sub>	0.08	<0.02	<0.02	0.05	0.10	0.03
Total	99.80	99.90	99.28	99.38	100.19	99.93
2 oxygen atoms, apfu						
Si	0.962	0.957	0.965	0.973	0.969	0.974
Ti	0.002	0.002	0.003	0.003	0.001	0.002
Al	0.032	0.041	0.028	0.021	0.028	0.023
Fe	0.011	0.002	0.011	0.003	0.007	0.003
Mg	0.002	0.001	0.004	0.001	0.006	0.004
Ca	0.003	0.013	0.002	0.007	0.001	0.001
Na	0.006	0.010	0.007	0.006	0.006	0.006
K	0.009	0.000	0.001	0.004	0.001	0.002
P	0.001	0.000	0.000	0.000	0.001	0.000
Total	1.026	1.026	1.022	1.017	1.019	1.016

apfu = atoms per formula unit; MnO < 0.06 wt%.

**Table 8.** Mineral chemistry of intermediate members of the magnetite–ulvöspinel solid solutions and ilmenite from combustion metamorphic rocks of Karabetova Gora MV. EPMA data (in wt%).

Mineral	Intermediate Members of the Magnetite–Ulvöspinel Solid Solutions			Ilmenite
	1	2	3	
Analysis no.				4
SiO <sub>2</sub>	0.50	0.45	0.42	0.45
TiO <sub>2</sub>	12.12	11.00	12.69	48.56
Al <sub>2</sub> O <sub>3</sub>	13.29	5.50	4.18	2.43
FeO *	41.77	38.62	40.47	43.55
Fe <sub>2</sub> O <sub>3</sub> *	28.22	41.54	38.03	
MnO	0.57	0.38	0.38	0.87
MgO	0.66	2.00	1.01	3.15
CaO	1.19	0.67	0.95	0.09
Total	98.31	100.16	98.14	99.10
		3 cations, apfu		
Si	0.018	0.016	0.016	
Ti	0.325	0.300	0.357	
Al	0.558	0.235	0.184	
Fe <sup>3+</sup>	0.757	1.133	1.070	
Fe <sup>2+</sup>	1.245	1.170	1.266	
Mn	0.017	0.012	0.012	
Mg	0.035	0.108	0.056	
Ca	0.045	0.026	0.038	

apfu = atoms per formula unit; FeO \* and Fe<sub>2</sub>O<sub>3</sub> \* are calculated by charge balance.

#### 4.3. Numerical Simulation Results

The giant 300–400 m high short-lived gas flare that arose during the catastrophic eruption of Karabetova Gora MV on 6 May 2000 was simulated assuming the following boundary conditions: combustible gas vents into the atmosphere from a conduit 4 m in diameter and ignites on the ground surface; the starting gas temperature and ambient temperature is 25 °C; ground temperature at 30 m below the surface is 5 °C; no high-temperature ( $T > 500$  °C) halo forms around the vent. The calculations were performed using different flow rates of combustible gas and CH<sub>4</sub>:CO<sub>2</sub> ratios. Note that the presence of up to 15 vol% CO<sub>2</sub> in the gas mixture did not cause significant effects on the simulation results.

The version of calculations for 250 kg/s methane flow rate was the closest to the real flare parameters (Figure 8). When gas emission was faster than flame propagation, the flame front detached from the origin of the gas gusher and became suspended at some height above the ground. According to our calculations, the flame detached at a height of 10 m at the 250 kg/s gas flow rate. The zone of highest temperatures inside the flare (~1400–1540 °C) was located at heights between 75 and 250 m. The heat flux to the ground in this case was mainly radiative and decreased rapidly. The maximum radiative flux density was estimated to reach 16.7 kW/m<sup>2</sup>, while the highest ground surface temperature immediately beneath the flare did not exceed 280 °C.

The exact lifespan of the flare being unknown for the lack of eye witness reports, the calculations were performed assuming that gas was burning for 15 min, which is a typical duration for such flare parameters [16,17]. The estimated volume of combusted gas (CH<sub>4</sub>) was 346,500 m<sup>3</sup> (225 tons) for cold gas (normal conditions) or ~2,000,000 m<sup>3</sup> (at 1540 °C gas temperature in the flare center).

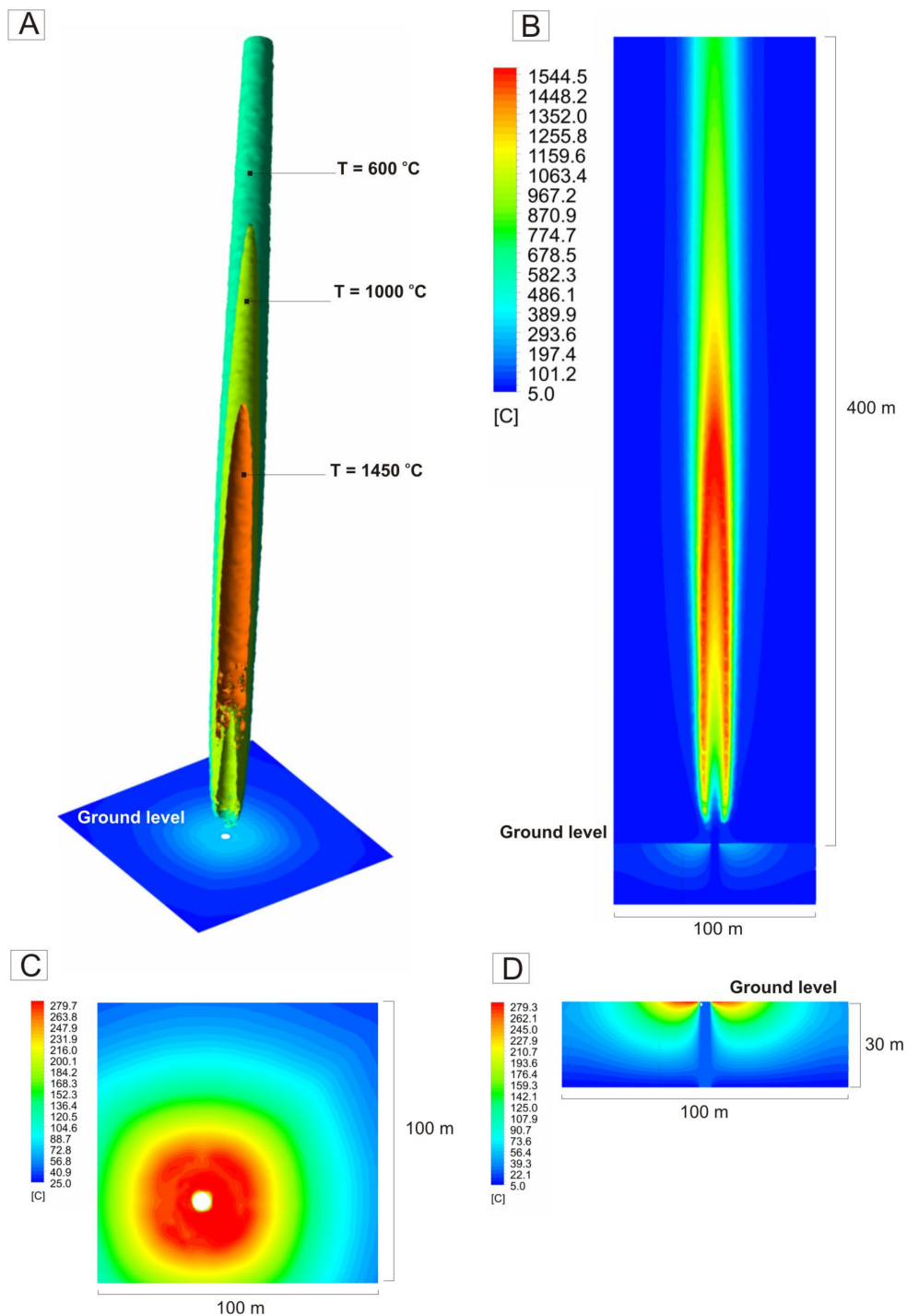


**Figure 8.** Natural straight-flow vertical gas flare and its temperature pattern. (A) Color-coded isothermal surfaces: blue, green, and red colors correspond to temperatures of 600, 1000, and 1450 °C, respectively, and ground temperatures (°C). (B–D) Temperature fields (°C) in the central section (B), on ground surface (C), and to 30 m below the surface (D).

## 5. Discussion

### 5.1. Combustion Metamorphism: Processes and Products

Combustion metamorphism is a type of thermal metamorphism involving very high temperatures often to the point of causing melting at very low (often ambient) pressure. Nominally CM rocks were classified by Callegari and Pertsev [40] and by Grapes [11] as sanidinite facies contact metamorphics but making a particular genetic group due

to an unusual heat source. Combustion metamorphic or pyrometamorphic (annealed, melted, and slag-like) rocks are produced by in situ natural combustion of fossil fuels and are typical geological features in many coal deposits, some oil basins, and regions of bituminous sedimentation. High-temperature (up to 1000 °C) and especially ultrahigh-temperature (1200–1500 °C), low pressure thermal effects are usually restricted to very narrow spots heated and/or melted by burning gas [7,14,25,53]. Such CM varieties, and even enormous amounts of molten and quenched rocks, formed sometimes in the Late Cenozoic in zones where bitumen in sediments and gas were burning together or where burning occurred within gas traps [4,53–55].

Fossil fuel combustion as a specific heat source that causes CM alteration of sediments has several features: (1) an abrupt temperature rise to 1000–1500 °C in the flame zone; (2) convective heat and mass transfer; (3) pyrolysis and in situ gasification of solid fuel in the zone of restricted oxygen flow. Such heat sources create extremely high temperature gradients with variations of hundreds °C over a few meters or even centimeters [5,7,11,14,16,17,25]. The thermal impact of short to extremely short duration creates a unique mineral-forming environment: rapid decomposition of precursor sedimentary minerals, delamination and dihydroxylation of phyllosilicates, degassing, metastable melting, and growth of high-temperature minerals driven by significant temperature overstepping of equilibrium conditions. Although being of far more limited occurrence than other metamorphic facies, CM rocks are remarkable in a particular phase composition with crystalline and amorphous phases. The latter include thermally decomposed precursor phases in lower temperature assemblages and glasses in higher-temperature ones. The particular compositions (assemblages of minerals, glasses, and amorphous phases), textures, and crystal habits result from the effects of high temperature and chemical disequilibrium caused by incomplete reaction due to rapid heating and quenching. Generally, the distribution patterns of phases, as well as the specific morphology of quench solids (skeletal or hopper-like crystals, clasts of laths in glass), and the alignment of crystals around vesicles are common to paralava, iron sinter, and smelter slag, which indicates rapid crystallization from a melt [6,10,11].

Ultrahigh-temperature CM alteration is marked by (i) the presence of glass in pelitic lithologies; (ii) unusual melt compositions produced by bulk melting of dehydrated and decarbonated sediments along with melts compositionally similar to anhydrous silicate eutectic melts; and (iii) crystallization of minerals from anhydrous melts and their quenching morphology. The paralavas are generally characterized by large variety of textures and non-hydroxyl-bearing high-temperature minerals, including quench crystals of tridymite, low-silica plagioclase, potassium feldspar, fayalite, ortho- and clinopyroxenes, wollastonite, mullite, gehlenite-rich melilite solid solutions, Fe-bearing cordierite, and Fe- and Al-rich spinel. The paralava glass formed by very rapid quenching looks felt-like or becomes a structureless matrix impregnated with abundant tiny grains of anhydrous silicates and opaque minerals [4,6,10,11,15,20,41].

At moderate temperatures ( $T < 900$  °C) or at a brief contact with rapidly dissipated hot gas, the metasedimentary substrate does not melt, but primary H<sub>2</sub>O- or (OH)-bearing minerals become dehydrated and dehydroxylated, whereby the precursor phyllosilicates decompose to a mixture of amorphous compounds. The processes of long-range disordering coupled with water loss are known as amorphization [11]. The CM alteration occurring at  $T < 900$  °C also includes (i) decomposition of carbonate minerals; (ii) generation of intergranular melt films in pelitic lithologies; (iii) peripheral fusion of grains, and related induration of the heated rocks; and (iv) oxidation of iron and related reddening of iron-enriched (siderite- or pyrite-bearing) rocks [11,20,41]. These rocks preserve only detrital quartz intact and resemble bricks in appearance, mode of formation, and strength, and are commonly classified as red clinker.

To sum up, the strong overheating (especially from burning gas), high viscosity of dry Ca-depleted, Al-rich silicate melts, and extremely rapid quenching of heated or melted compounds after the instantaneous flare extinguishing leaves no chance for the CM rocks to

develop equilibrium assemblages [11]. This is a prominent feature of ultrahigh-temperature Al- and Si-rich CM rocks produced by gas fires. Therefore, such systems often step over the mineral equilibrium lines and the related assemblages lack many phases that would appear in slower (quasi-equilibrium) processes. The probability of phase transitions and the sequence of crystallization are controlled in this case by the kinetics of the process (Ostwald step rule) rather than by thermodynamics [11].

### 5.2. Regime of Combustion Metamorphism Caused by MV Fire Eruptions

The obtained data from the Karabetova Gora MV site have petrogenetic implications for mud exposed to the thermal impact of a gas flare. Bulk melting of the dehydrated pelitic protolith was limited to a 3–5 mm rim near the surface of blocks or locally produced flow structures, while spot melting was traceable until 1.5 cm below the surface. In addition to anhydrous Al-silicate glass, we identified in the Karabetova Gora CM rocks high-temperature, low-pressure index minerals, such as tridymite, cristobalite, and mullite in melt rocks, which taken together, they reveal the sanidinite facies conditions of metamorphism. The mineralogical conclusions are supported by the SigmaFlow numerical simulation of temperature (1400–1540 °C) for the flare core (Figure 8) and the known ambient pressure.

The impact of the ultrahigh-temperature heat pulse already decayed rapidly 2 cm below the surface of the annealed blocks where mud breccia remained unmolten and preserved its original texture. Judging by the preservation of quartz and feldspar, the temperature was no higher than 870 °C. The principal high-temperature processes in the 2 cm outer zone below the molten crust included solid-phase clinkering and recrystallization of dehydrated and dehydroxylated amorphous Al-silicate matter. The heat pulse produced a high temperature gradient (at least 250 °C/cm) within 2 cm below the surface in the target material, which apparently changed in a nonlinear way and was the greatest near the surface. High redox gradients were additionally inferred from the presence of ferrous spinel coexisting with ferrous pyroxene and cordierite in the molten outer zone, as well as the preservation of authigenic pyrite at a depth of 2.5 cm.

The CM products of the Karabetova Gora MV eruption are remarkable by prominent heterogeneity even within 0.3 mm × 0.3 mm molten spots: different phase compositions in neighboring spots and diversity of newly formed silicates and glasses. The fast cooling of vitreous samples was confirmed further by typical quench morphology of newly formed phases, as well as by mosaic distribution of high-temperature mineral assemblages (Figures 5–7). The thermally altered rock is actually a snapshot of micro-variations in the protolith composition. Anhydrous and Ca-poor silicate CM melts failed to become compositionally homogeneous due to their high viscosity ( $10^{2.0}$ – $10^{2.3}$  Pa·s;  $T = 1400$  °C; calculated using the method of Persikov and Bukhtiyarov [56]) and the brevity of exposure to ultrahigh temperatures. Furthermore, both factors impeded crystallization of solids and glass devitrification. Indeed, the total amount of newly formed high-temperature crystalline phases in the Karabetova Gora paralavas was as low as 10–21 wt% (Table 2).

The timescale of the exposure to burning gas is impossible to estimate exactly, but possible bounds are justifiable. The rocks were exposed to the gas flare for a few seconds (a few tens of seconds at most), from the firing time (explosion) until the time when the block fell on the ground. The heat dissipation timescales for the molten outer zone and the thermally affected interior were apparently different: the former was likely air quenched mode [57,58], whereas the block interior under the insulating quenched coat was cooling down for a few hours. Heating at such high rates ( $\geq 100$  K/s) is classified as a thermal shock in the respective technological protocols. Thus, the outer zone of the blocks actually underwent a thermal shock, with instantaneous inhomogeneous heating, which produced high temperature gradients.

The phase and textural heterogeneity of the Karabetova Gora CM rocks provide strong evidence of local disequilibria in the system. The SigmaFlow numerical simulation yielded an estimate of 1400–1540 °C for the flare core (Figure 8), while the 1500–1800 °C maximum

temperature of methane burning in air [59] can be considered as the upper temperature limit. The target material surface reached these temperatures for a few seconds at the longest. Therefore, any direct analogy with experimentally investigated petrological and technological (mainly ceramic) systems requires much caution in this case.

### 5.3. Was the Karabetova Gora MV Gas Flare a Highly Energetic Fast Geological Event?

Melting triggered by CM ultrahigh-temperature events is a non-equilibrium process which differs substantially from equilibrium magma generation. All magmatic melts are formed slowly at relatively low temperatures and correspond to eutectic compositions, whereas the natural CM events triggered by gas fires are extremely brief, and their culmination (up to 1500 °C) lasts at least a few seconds [16,17]. Unlike the slow magma generation, the rapid temperature rise at fire foci leads to the formation of non-eutectic melts compositionally similar to the bulk devolatilized sedimentary protolith [4,11,15,20]. In this respect, the Karabetova melt rocks are typical ultrahigh-temperature CM varieties. Non-equilibrium bulk melting of target materials on the ground surface can result from yet another brief ultrahigh-temperature, low-pressure natural event: lightning-induced terrestrial pyrometamorphism, which produces fulgurites [41]. It is a highly energetic, fast geological event, in which a huge amount of energy is supplied to the target systems in fractions of a second and the heating rates reach  $\geq 100$  K/s [60–62] at microsecond timescales [63]. Such an amount of heat is able to melt/vaporize inorganic materials and to cause volatilization of most of major elements and formation of melts enriched in silica and depleted in alkalis [41]. Extremely fast cooling of such melts produces homogeneous high-silica glass [60]. Fulgurites commonly enclose micrometer-size globules of reduced compounds of metals (Fe, Si), silicides (FeSi, Fe<sub>3</sub>Si<sub>7</sub>, FeTiSi<sub>2</sub>), and phosphides (TiP, Fe<sub>3</sub>P) coexisting with vesicular silica-rich (82–99 wt% SiO<sub>2</sub>) glass, residual undermolten quartz, and graphite [11,63]. However, the Karabetova CM rocks differ from fulgurites as the protolith only lost Na and Si, the redox conditions in the mineral-forming medium were oxidative, and Fe<sup>2+</sup>- and Fe<sup>3+</sup>-bearing oxygenated compounds were formed instead of native elements, phosphides, or silicides. The highest-temperature stage of the Karabetova CM event triggered by gas combustion was six orders of magnitude longer than lightning-induced melting. Thus, the obvious difference of Karabetova paralavas from fulgurites does not allow interpreting the gas fire-related pyrometamorphism as a highly energetic fast geological event.

The compared mineral-forming systems contain specific sets of chemical compounds. Annealed and fused metapelitic CM rocks tend to lose more than 90% of volatiles and up to 2/3 Na, but not potassium. As a result, CM melts are K-Al silica-rich and crystallize to form anhydrous Na-depleted mineral assemblages, mostly simple anhydrous oxides and silicates of major elements (Si, Al, Fe, Mg, Ca, Ti, K). In the known ordinary cases of natural and human-induced coal fires, CM assemblages are formed in the conditions of (i) high temperature, low pressure, and heating duration from several months to several years in any local spot; (ii) high chemical heterogeneity of sedimentary protoliths; (iii) gas convection; and (iv) high temperature and redox gradients. Jointly, these conditions lead to the formation of exceptionally diverse prograde CM mineral assemblages. They are especially diverse in hybrid rocks resulting from high-temperature alteration of carbonate and pelitic substrates, marly and phosphatic sediments with high trace-element loading, as well as molten rocks and assemblages of gas transport in gas chimneys. In these cases, a lot of minor and trace elements (F, Cl, P, S, Se, As, Sr, Ba, Zn, Cd, Cr, Ni, Mn, Mo, U, Pb, Ce, Th, Zr, Sn) become important mineral-forming agents besides the major elements (O, Si, Al, Fe, Mg, Ca, Ti, K, and rarer Na), and yield numerous combinations from bi-element to six-element compounds [13,15,20,26,50,55,64–67].

Contrary to these highly productive systems, the mineralogical productivity of the Karabetova Gora metapelitic CM rocks (Figure 9) was as low as 1.38 ( $K = M_{\text{minerals}} / N_{\text{elements}} = 11/8$ ), and is one of lowest among all CM rock samples in this study and in published evidence [13,14,16,17,55]. The low mineralogical diversity is due to narrow

ranges of formation conditions and protolith compositions (monotonic shales), as well as to polymerization of dry high-silica melts during quenching. The mineralogy of the Karabetova Gora CM rocks includes only oxygenated compounds, mostly bi- or three-element: three species of oxides (Si-O and Fe-O), three species of double oxides (Fe-Ti-O and Mg-Fe-O), and one simple Al silicate (Al-Si-O). Four mineral species consist of five elements, all silicates: pigeonite (Ca-Mg-Fe-Si-O), cordierite (Mg-Fe-Al-Si-O), labradorite, and bytownite (Ca-Na-Al-Si-O).

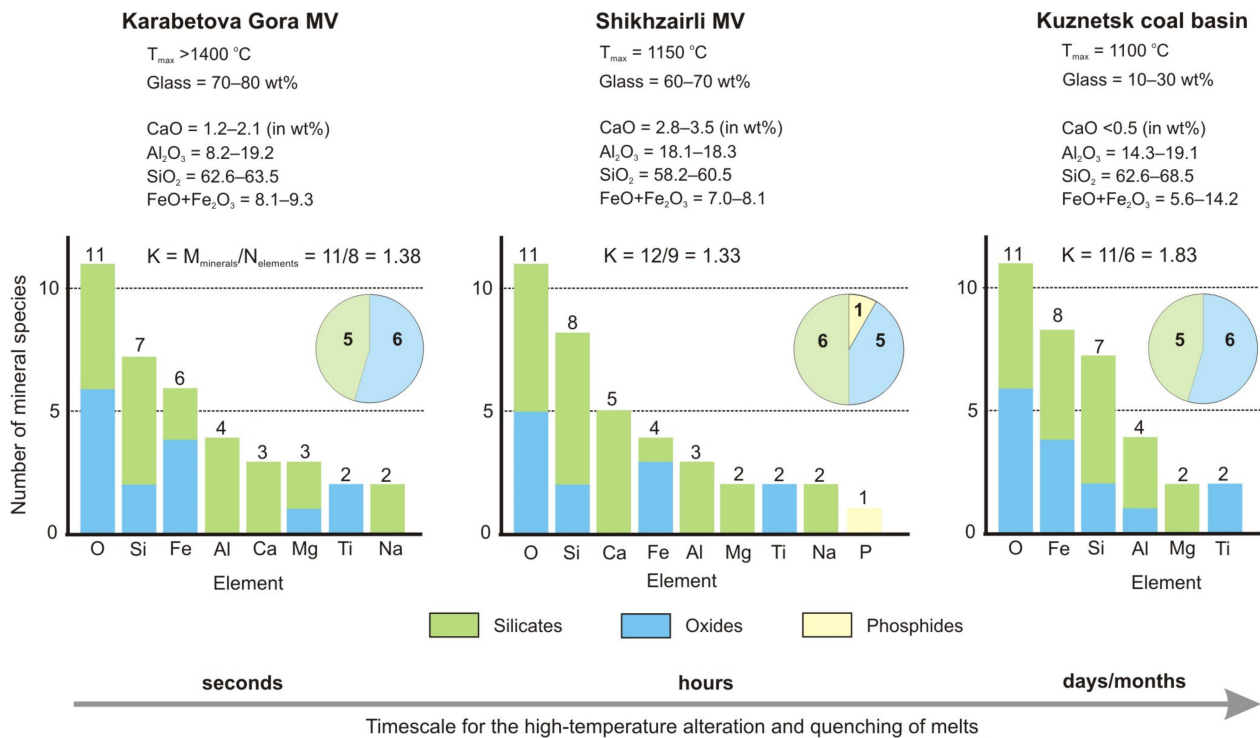


**Figure 9.** Mineralogical diversity of metapelitic CM rocks produced by Karabetova Gora MV fire eruption and productivity of elements. Compared are compositionally similar metapelitic CM rocks genetically related to Shikhzairli MV gas fire [17] and Kuznetsk basin coal fire [12].

Importantly, CM alteration of low-Ca clayey protoliths in the three compositionally similar mineral-forming systems differs markedly in the duration of the high-temperature stage, as well as in the rates of melt cooling and quenching (Figure 9). As the duration of the thermal impact increases from seconds (Karabetova Gora MV) to hours (Shikhzairli MV) and on to days/months (Kuznetsk coal basin), crystalline phases in CM rocks form in progressively higher percentages, while the amount of glass decreases from 70–80 wt% to 10–30 wt%. The mineralogical productivity is the highest ( $K = 1.8$ ) in CM rocks formed in coal fires (Kuznetsk Coal Basin) but is low ( $K \sim 1.3$ ) in those from both Karabetova Gora and Shikhzairli MVs produced by brief events. The inverse correlation of mineralogical productivity in CM rocks with duration of high-temperature events indicates that it is kinetically controlled in fast ultrahigh-temperature events. In this respect, mineralogical productivity can be a proxy of CM event duration for compositionally similar CM rocks.

Thus, the natural thermal events such as onshore MV fire eruptions and their products have their specificity. Although being extremely short (second-to-minute timescales) and high-temperature (up to  $1500\text{ }^{\circ}\text{C}$ ), they are yet inferior to highly energetic fast geological events that last a few milliseconds and reach a temperature of  $2000\text{ K}$  [11,41]. Meanwhile, catastrophic offshore MV fire eruptions are still shorter than other ultrahigh-temperature natural CM events. Some events of this kind leave a “foam” consisting of hollow glass microspheres, like those floating on the surface of the Caspian Sea, known under the name “lapilli” [68]. They arise by the same mechanism as microspheres in fly ash at thermal

power plants [69,70]: bulk melting of dispersed mud drops in giant (400–500 m height) gas flares that are quenched in sea water. This extreme CM process may be the closest to highly energetic fast geological events.

## 6. Conclusions

The reported data on petrography, mineralogy, and mineral chemistry of the Karabetova Gora CM rocks, as well as the numerical simulation results for the burning gas gusher have led to several inferences.

- (1) The Karabetova Gora CM rocks formed under extreme CM conditions of a burning gas gusher, very similar to those of a thermal shock: ultrafast (within tens of seconds) high-temperature (1400–1540 °C) melting and quenching.
- (2) The CM rocks are remarkable by phase and texture heterogeneity caused by extremely high temperature gradients, brevity of the thermal shock, and high viscosity of dry, highly polymerized silicate melts.
- (3) The thermally altered clayey sediments were composed mainly of glass (70–80 wt%), while the total percentage of newly formed high-temperature crystalline phases, mostly ferrous spinel and silicates, was within 10–21 wt%. The glass also enclosed unmolten relict detrital grains of quartz (up to 16 wt%). The modest mineralogical diversity limited to eleven mineral species was due to the low-Ca protolith composition, as well as to a very specific CM alteration regime. The heating of the target rocks under the thermal shock conditions was fast enough to induce overstepping in a few mineral reactions/equilibria, which prevented the formation of stable phases but favored melting and subsequent vitrification upon cooling, rather than the growth of solids.

**Supplementary Materials:** The following supporting information can be downloaded at: <https://www.mdpi.com/article/10.3390/min13030355/s1>, Figure S1: The XRD patterns of the sedimentary protolith (a) and CM rocks: slightly annealed rock (b), clinker (c), and paralava (d).

**Author Contributions:** Project idea: S.N.K.; Conceptualization, S.N.K. and E.V.S.; field work, E.V.S. and S.N.K.; analytical work, E.V.S.; interpretation of analytical data, S.N.K. and E.V.S.; visualization, S.N.K.; writing, S.N.K. and E.V.S. All authors have read and agreed to the published version of the manuscript.

**Funding:** The study was carried out as part of a government assignment to the V.S. Sobolev Institute of Geology and Mineralogy (Novosibirsk, Russia).

**Data Availability Statement:** Not applicable.

**Acknowledgments:** We wish to thank P. V. Khvorov (South Urals Federal Research Center of Mineralogy and Geocology, Miass), A. A. Dekterev (Kutateladze Institute of Thermophysics, Novosibirsk), and T. I. Perepelova (NSU, Novosibirsk) for their helpful advice. We thank the anonymous reviewers for their valuable comments and suggestions.

**Conflicts of Interest:** The authors declare no conflict of interest.

## References

1. Clemens, J.D.; Vielzeuf, D. Constraints on melting and magma production in the crust. *Earth Planet. Sci. Lett.* **1987**, *86*, 287–306. [[CrossRef](#)]
2. Holtz, F.; Johannes, W. Genesis of peraluminous granites I. Experimental investigation of melt compositions at 3 and 5 kbar and various H<sub>2</sub>O activities. *J. Petrol.* **1991**, *32*, 935–958. [[CrossRef](#)]
3. Clemens, J.D. Partial melting and granulite genesis: A partisan overview. *Precambrian Res.* **1992**, *55*, 297–301. [[CrossRef](#)]
4. Bentor, Y.K.; Kastner, M.; Perlman, I.; Yellin, Y. Combustion metamorphism of bituminous sediments and the formation of melts of granitic and sedimentary composition. *Geochim. Cosmochim. Acta* **1981**, *45*, 2229–2255. [[CrossRef](#)]
5. Cosca, M.A.; Essene, E.J.; Geissman, J.W.; Simmons, W.B.; Coates, D.A. Pyrometamorphic rocks associated with naturally burned coal beds, Powder River Basin, Wyoming. *Am. Mineral.* **1989**, *74*, 85–100.
6. Kalugin, I.A.; Tretyakov, G.A.; Bobrov, V.A. *Iron Ore Basalts in Burned Rocks of Eastern Kazakhstan*; Publishing House Nauka: Novosibirsk, Russia, 1991; 80p. (In Russian)

7. Sokol, E.; Novikov, I.; Zateeva, S.; Vapnik, Y.; Shagam, R.; Kozmenko, O. Combustion metamorphism in Nabi Musa dome: New implications for a mud volcanic origin of the Mottled Zone, Dead Sea area. *Basin Res.* **2010**, *22*, 414–438. [[CrossRef](#)]
8. Sokol, E.V.; Kozmenko, O.A.; Kokh, S.N.; Vapnik, Y. Gas reservoirs in the Dead Sea area: Evidence from chemistry of combustion metamorphic rocks in Nabi Musa fossil mud volcano. *Russ. Geol. Geophys.* **2012**, *53*, 745–762. [[CrossRef](#)]
9. Sokol, E.V.; Novikova, S.A.; Alekseev, D.V.; Travin, A.V. Natural coal fires in the Kuznetsk Coal Basin: Geologic causes, climate, and age. *Russ. Geol. Geoph.* **2014**, *55*, 1043–1064. [[CrossRef](#)]
10. Sharygin, V.V.; Sokol, E.V.; Belakovsky, D.I. Mineralogy and origin of fayalite-sekaninaite paralava: Ravat coal fire, Central Tajikistan. In *Coal and Peat Fires: A Global Perspective*; Elsevier: Amsterdam, The Netherlands, 2015; Volume 3, pp. 582–607. [[CrossRef](#)]
11. Grapes, R. *Pyrometamorphism*, 2nd ed.; Springer: Berlin/Heidelberg, Germany, 2011; 365p.
12. Grapes, R.; Korzhova, S.; Sokol, E.; Seryotkin, Y. Paragenesis of unusual Fe-cordierite (sekaninaite)-bearing paralava and clinker from the Kuznetsk coal basin, Siberia, Russia. *Contrib. Miner. Petrol.* **2011**, *162*, 253–273. [[CrossRef](#)]
13. Grapes, R.; Sokol, E.; Kokh, S.; Kozmenko, O.; Fishman, I. Petrogenesis of Na-rich paralava formed by methane flares associated with mud volcanism, Altyn-Emel National Park, Kazakhstan. *Contrib. Miner. Petrol.* **2013**, *165*, 781–803. [[CrossRef](#)]
14. Seryotkin, Y.V.; Sokol, E.V.; Kokh, S.N. Natural pseudowollastonite: Crystal structure, associated minerals, and geological context. *Lithos* **2012**, *133–135*, 75–90. [[CrossRef](#)]
15. Stracher, G.B.; Prakash, A.; Sokol, E.V. (Eds.) *Coal and Peat Fires: A Global Perspective: Case Studies—Coal Fires*; Elsevier: Amsterdam, The Netherlands, 2015; Volume 3, 816p. [[CrossRef](#)]
16. Kokh, S.; Dekterev, A.; Sokol, E.; Potapov, S. Numerical simulation of an oil–gas fire: A case study of a technological accident at Tengiz oilfield, Kazakhstan (06.1985–07.1986). *Energy Explor. Exploit.* **2016**, *34*, 77–98. [[CrossRef](#)]
17. Kokh, S.N.; Sokol, E.V.; Dekterev, A.A.; Kokh, K.A.; Rashidov, T.M.; Tomilenko, A.A.; Bul’bak, T.A.; Khasaeva, A.; Guseinov, A. The 2011 strong fire eruption of Shikhzarli mud volcano, Azerbaijan: A case study with implications for methane flux estimation. *Environ. Earth Sci.* **2017**, *76*, 701. [[CrossRef](#)]
18. Burg, A.; Starinsky, A.; Bartov, Y.; Kolodny, Y. Geology of the Hatrurim Formation (“Mottled Zone”) in the Hatrurim Basin. *Isr. J. Earth Sci.* **1991**, *40*, 107–124.
19. Heffern, E.L.; Coates, D.A. Geological history of natural coal-bed fires, Powder River Basin, USA. *Coal Fires Burn. Around World Glob. Catastr. Int. J. Coal Geol.* **2004**, *59*, 25–47. [[CrossRef](#)]
20. Sokol, E.V.; Volkova, N.I. Combustion metamorphic events resulting from natural coal fires. In *GSA Reviews in Engineering Geology XVIII: Geology of Coal Fires: Case Studies from around the World*; Stracher, G.B., Ed.; The Geological Society of America: Boulder, CO, USA, 2007; pp. 97–115. [[CrossRef](#)]
21. Bagirov, E.; Lerche, I. Flame hazards in the South Caspian Basin. *Energy Explor. Exploit.* **1998**, *16*, 373–397. [[CrossRef](#)]
22. Kopf, A. Significance of mud volcanism. *Rev. Geophys.* **2002**, *40*, 1–52. [[CrossRef](#)]
23. Shnyukov, E.; Sheremetiev, V.; Maslakov, N.; Kutniy, V.; Gusakov, I.; Trofimov, V. *Mud Volcanoes of the Kerch-Taman Region*; GlavMedia Publishing House: Krasnodar, Russia, 2005; 176p. (In Russian)
24. Mazzini, A.; Etiope, G. Mud volcanism: An updated review. *Earth-Sci. Rev.* **2017**, *168*, 81–112. [[CrossRef](#)]
25. McLintock, W.E.P. On the metamorphism produced by the combustion of hydrocarbons in the Tertiary sediments of southwest Persia. *Mineral. Mag.* **1932**, *23*, 207–226. [[CrossRef](#)]
26. Gross, S. The mineralogy of the Hatrurim Formation. *Isr. Geol. Surv. Isr. Bull.* **1977**, *70*, 80.
27. Sokol, E.V.; Seryotkin, Y.V.; Kokh, S.N.; Vapnik, Y.; Nigmatulina, E.N.; Goryainov, S.V.; Belogub, E.V.; Sharygin, V.V. Flamite (Ca,Na,K)<sub>2</sub>(Si,P)O<sub>4</sub>, a new mineral from the ultrahigh-temperature combustion metamorphic rocks, Hatrurim Basin, Negev Desert, Israel. *Miner. Mag.* **2015**, *79*, 583–596. [[CrossRef](#)]
28. Rashchenko, S.V.; Sokol, E.V.; Seryotkin, Y.V.; Kokh, S.N. Incommensurately modulated crystal structure of flamite–natural analogue of  $\alpha'$ -H-Ca<sub>2</sub>SiO<sub>4</sub>. *Acta Crystallogr. Sect. B Struct. Sci. Cryst. Eng. Mater.* **2019**, *75*, 1137–1143. [[CrossRef](#)]
29. Kopf, A.; Deyhle, A.; Lavrushin, V.Y.; Polyak, B.G.; Gieskes, J.M.; Buachidze, G.I.; Wallmann, K.; Eisenhauer, A. Isotopic evidence (He, B, C) for deep fluid and mud mobilization from mud volcanoes in the Caucasus continental collision zone. *Int. J. Earth Sci. Geol. Rundsch.* **2003**, *92*, 407–425. [[CrossRef](#)]
30. Lavrushin, V.Y.; Aydarkozhina, A.S.; Sokol, E.V.; Chelnokov, G.A.; Petrov, O.L. Mud volcanic fluids of the Kerch–Taman region: Geochemical reconstructions and regional trends. Communication 1: Geochemical features and genesis of mud-volcanic waters. *Lithol. Miner. Resour.* **2021**, *56*, 461–486. [[CrossRef](#)]
31. Lavrushin, V.Y.; Aydarkozhina, A.S.; Sokol, E.V.; Chelnokov, G.A.; Petrov, O.L. Mud volcanic fluids of the Kerch–Taman region: Geochemical reconstructions and regional trends. Communication 2: Genesis of mud volcanic gases and regional geochemical trends. *Lithol. Miner. Resour.* **2022**, *57*, 1–24. [[CrossRef](#)]
32. Kokh, S.N.; Shnyukov, Y.F.; Sokol, E.V.; Novikova, S.A.; Kozmenko, O.A.; Semenova, D.V.; Rybak, E.N. Heavy carbon travertine related to methane generation: A case study of the Big Tarkhan cold spring, Kerch Peninsula, Crimea. *Sediment. Geol.* **2015**, *325*, 26–40. [[CrossRef](#)]
33. Kokh, S.N.; Sokol, E.V.; Gustaytis, M.A.; Sokol, I.A.; Deviatiiarova, A.S. Onshore mud volcanoes as a geological source of mercury: Case study from the Kerch Peninsula, Caucasus continental collision zone. *Sci. Total Environ.* **2021**, *751*, 141806. [[CrossRef](#)]
34. Kokh, S.N.; Sokol, E.V.; Gustaytis, M.A. Mercury anomaly in Oligocene-Miocene Maykop Group sediments (Caucasus continental collision zone): Mercury hosts, distribution, and sources. *Minerals* **2021**, *11*, 751. [[CrossRef](#)]

35. Sokol, E.; Kokh, S.; Kozmenko, O.; Novikova, S.; Khvorov, P.; Nigmatulina, E.; Belogub, E.; Kirillov, M. Mineralogy and geochemistry of mud volcanic ejecta: A new look at old issues (a case study from the Bulganak field, Northern Black Sea). *Minerals* **2018**, *8*, 344. [\[CrossRef\]](#)
36. Sokol, E.V.; Kokh, S.N.; Kozmenko, O.A.; Lavrushin, V.Y.; Belogub, E.V.; Khvorov, P.V.; Kikvadze, O.E. Boron in an onshore mud volcanic environment: Case study from the Kerch Peninsula, the Caucasus continental collision zone. *Chem. Geol.* **2019**, *525*, 58–81. [\[CrossRef\]](#)
37. Kikvadze, O.E.; Lavrushin, V.Y.; Polyak, B.G. Chemical geothermometry: Application to mud volcanic waters of the Caucasus region. *Front. Earth Sci.* **2020**, *14*, 738–757. [\[CrossRef\]](#)
38. Kharaka, Y.K.; Mariner, R.H. Chemical Geothermometers and Their Application to Formation Waters from Sedimentary Basins. In *Thermal History of Sedimentary Basins. Methods and Case Histories*; Naeser, N.D., McCulloh, T.H., Eds.; Springer: New York, NY, USA, 1989; pp. 99–117.
39. Smyslov, A.A. *Geothermal Map: Map of the Crustal Heat Flow Regime in the USSR Territory. Scale 1:10,000,000*; Ministry of Geology: Moscow, Russia, 1977. (In Russian)
40. Callegari, E.; Pertsev, N. Contact metamorphic and associated rocks. In *Metamorphic Rocks: A Classification and Glossary of Terms*; Fettes, D., Desmons, J., Eds.; Cambridge University Press: New York, NY, USA, 2007; pp. 69–81.
41. Cicconi, M.R.; McCloy, J.S.; Neuville, D.R. Non-magmatic glasses. *Rev. Mineral. Geochem.* **2022**, *87*, 965–1014. [\[CrossRef\]](#)
42. Shatsky, V.; Sitnikova, E.; Kozmenko, O.; Palessky, S.; Nikolaeva, I.; Zayachkovsky, A. Behavior of incompatible elements during ultrahigh-pressure metamorphism (by the example of rocks of the Kokchetav massif). *Russ. Geol. Geophys.* **2006**, *47*, 482–496.
43. Jeffery, P.G. *Chemical Methods of Rock Analysis*; Pergamon Press: Oxford, UK; New York, NY, USA, 1970; 507p.
44. Hubert, F.; Caner, L.; Meuner, A.; Ferrage, E. Unraveling complex <2 μm clay mineralogy from soils using X-ray diffraction profile modeling on particle-size sub-fractions: Implications for soil pedogenesis and reactivity. *Am. Mineral.* **2012**, *97*, 384–398. [\[CrossRef\]](#)
45. Kamenschikov, L.P.; Bykov, V.I.; Dektarev, A.A.; Kovalevsky, A.M. Simulation of reacting turbulent flows in 3D domains of complex geometry. *Khimicheskaya Prom.* **1995**, *1*, 43–47. (In Russian)
46. Dektarev, A.A.; Gavrilov, A.A.; Minakov, A.V. Advanced options of the SigmaFlow CFD code for thermophysical applications. *Sci. Today Res. Ideas Results Technol.* **2010**, *2*, 117–122. (In Russian)
47. Sokol, E.; Volkova, N.; Lepezin, G. Mineralogy of pyrometamorphic rocks associated with naturally burned coal-bearing spoil-heaps of the Chelyabinsk coal basin, Russia. *Eur. J. Mineral.* **1998**, *10*, 1003–1014. [\[CrossRef\]](#)
48. Sharygin, V.V.; Sokol, E.V.; Nigmatulina, E.N.; Lepezin, G.G.; Kalugin, V.M.; Frenkel, A.E. Mineralogy and petrography of technogenic parbasalts from the Chelyabinsk brown-coal basin. *Geol. Geofiz.* **1999**, *6*, 896–915.
49. Sokol, E.; Sharygin, V.; Kalugin, V.; Volkova, N.; Nigmatulina, E. Fayalite and kirschsteinite solid solutions in melts from burned spoil-heaps, South Urals, Russia. *Eur. J. Mineral.* **2002**, *14*, 795–807. [\[CrossRef\]](#)
50. Žáček, V.; Skála, R. Mineralogy of burning-coal waste piles in collieries of the Czech Republic. In *Coal and Peat Fires: A Global Perspective*; Elsevier: Amsterdam, The Netherlands, 2015; Volume 3, pp. 109–159. [\[CrossRef\]](#)
51. Schreyer, W.; Maresch, W.V.; Daniels, P.; Wolfsdorff, P. Potassic cordierites: Characteristic minerals for high-temperature, very low-pressure environments. *Contrib. Mineral. Petrol.* **1990**, *105*, 162–172. [\[CrossRef\]](#)
52. Sokol, E.V.; Nigmatulina, E.N.; Volkova, N.I. Fluorine mineralisation from burning coal spoil-heaps in the Russian Urals. *Mineral. Petrol.* **2002**, *75*, 23–40. [\[CrossRef\]](#)
53. Sokol, E.V.; Novikov, I.S.; Zateeva, S.N.; Sharygin, V.V.; Vapnik, Y. Pyrometamorphic rocks of the spurrite-merwinite facies as indicators of hydrocarbon discharge zones (the Hatrurim Formation, Israel). *Dokl. Earth Sci.* **2008**, *420*, 608–614. [\[CrossRef\]](#)
54. Sokol, E.V.; Kokh, S.N.; Vapnik, Y.; Thiery, V.; Korzhova, S.A. Natural analogs of belite sulfoaluminate cement clinkers from Negev Desert, Israel. *Am. Mineral.* **2014**, *99*, 1471–1487. [\[CrossRef\]](#)
55. Sokol, E.V.; Kokh, S.N.; Sharygin, V.V.; Danilovsky, V.A.; Seryotkin, Y.V.; Liferovich, R.; Deviatiarova, A.S.; Nigmatulina, E.N.; Karmanov, N.S. Mineralogical Diversity of Ca<sub>2</sub>SiO<sub>4</sub>-Bearing Combustion Metamorphic Rocks in the Hatrurim Basin: Implications for Storage and Partitioning of Elements in Oil Shale Clinkering. *Minerals* **2019**, *9*, 465. [\[CrossRef\]](#)
56. Persikov, E.S.; Bukhtiyarov, P.G. Viscosity of magmatic melts: Improved structural-chemical model. *Chem. Geol.* **2020**, *556*, 119820. [\[CrossRef\]](#)
57. Chawla, K.K. *Ceramic Matrix Composites*; Springer: Boston, MA, USA, 2003; 441p. [\[CrossRef\]](#)
58. Hetnarski, R.B. *Encyclopedia of Thermal Stresses*; Springer: Dordrecht, The Netherlands, 2014; pp. 5083–5167. [\[CrossRef\]](#)
59. Lewis, B.; von Elbe, G. *Combustion, Flames and Explosions of Gases*, 3rd ed.; Academic Press Inc.: Orlando, FL, USA, 1987; 739p. [\[CrossRef\]](#)
60. Grapes, R.H.; Müller-Sigmund, H. Lightning-strike fusion of gabbro and formation of magnetite-bearing fulgurite, Cornone di Blumone, Adamello, Western Alps, Italy. *Mineral. Petrol.* **2010**, *99*, 67–74. [\[CrossRef\]](#)
61. Pasek, M.A.; Block, K.; Pasek, V. Fulgurite morphology: A classification scheme and clues to formation. *Contrib. Mineral. Petrol.* **2012**, *164*, 477–492. [\[CrossRef\]](#)
62. Sengupta, P. Natural glasses under extreme conditions. In *Materials under Extreme Conditions*; Tyagi, A.K., Banerjee, S., Eds.; Elsevier: Amsterdam, The Netherlands, 2017; pp. 235–258.
63. Feng, T.; Abbatiello, J.; Omran, A.; Mehta, C.; Pasek, M.A. Iron silicides in fulgurites. *Minerals* **2021**, *11*, 1394. [\[CrossRef\]](#)

64. Lapham, D.M.; Barnes, J.H.; Downey, W.F.; Finkelman, R.B. *Mineralogy Associated with Burning Anthracite Deposits in Eastern Pennsylvania*; Mineral Resource Report 78; Pennsylvania Geological Survey: Harrisburg, PA, USA, 1980; 82p.
65. Chesnokov, B.V.; Shcherbakova, E.P.; Nishanbaev, T.P. *Minerals from Burned Dumps of Chelyabinsk Coal Basin*; Ural Branch of Russian Academy of Sciences, Institute of Mineralogy: Miass, Russia, 2008; 139p. (In Russian)
66. Hazen, R.M.; Morrison, S.M. On the paragenetic modes of minerals: A mineral evolution perspective. *Am. Mineral.* **2022**, *107*, 1262–1287. [[CrossRef](#)]
67. Hazen, R.M.; Morrison, S.M.; Krivovichev, S.V.; Downs, R.T. Lumping and splitting: Toward a classification of mineral natural kinds. *Am. Mineral.* **2022**, *107*, 1288–1301. [[CrossRef](#)]
68. Aliev, A.A.; Guliyev, I.S.; Rakhmanov, R.R. *Catalogue of Mud Volcano Eruptions of Azerbaijan (1810–2007 Years)*; Nafta-Press: Baku, Azerbaijan, 2009; p. 110.
69. Sokol, E.V.; Maksimova, N.V.; Volkova, N.I.; Nigmatulina, E.N.; Frenkel, A.E. Hollow silicate microspheres from fly ashes of the Chelyabinsk brown coals (South Urals, Russia). *Fuel Process. Technol.* **2000**, *67*, 35–52. [[CrossRef](#)]
70. Sokol, E.V.; Kalugin, V.M.; Nigmatulina, E.N.; Frenkel, A.E.; Maksimova, N.V. Ferrospheres from fly ashes of Chelyabinsk coals: Chemical composition, morphology and formation conditions. *Fuel* **2002**, *81*, 867–876. [[CrossRef](#)]

**Disclaimer/Publisher’s Note:** The statements, opinions and data contained in all publications are solely those of the individual author(s) and contributor(s) and not of MDPI and/or the editor(s). MDPI and/or the editor(s) disclaim responsibility for any injury to people or property resulting from any ideas, methods, instructions or products referred to in the content.